# ZEB1 controls a lineage-specific transcriptional program essential for melanoma cell state transitions

Yaqi Tang[1,§], Simon Durand[1,§], Roxane M. Pommier[2], Valentin Benboubker[1], Maxime Grimont[1], Eric Cumunel[2], Felix Boivin[1], Florian Dupeuble[1], Laetitia Barbollat-Boutrand[1], Anaïs Eberhardt[1,3], Maud Plaschka[1], Stéphane Dalle[1,3], Julie Caramel[1,*].

[1] Cancer Research Center of Lyon, Université de Lyon, Université Claude Bernard Lyon 1, INSERM 1052, CNRS 5286, Centre Léon Bérard, "Cancer cell Plasticity in Melanoma" team.

[2] Fondation Synergie Lyon Cancer, Plateforme de bio-informatique Gilles Thomas, Centre Léon Bérard, Lyon, France.

[3] Dermatology Unit, Hospices Civils de Lyon, CH Lyon Sud, 165 chemin du Grand Revoyet, 69495 Pierre Bénite Cedex, France.

§Contributed equally

*Correspondence: julie.caramel@lyon.unicancer.fr

**Running title:** ZEB1 transcriptional function in melanoma

**Keywords:** melanoma; plasticity; intra-tumor heterogeneity; transcription factor; ChIP-sequencing; neural-crest stem cell state; single-cell spatial multiplexed analyses

**Financial support**: This work was funded by the Ligue Nationale contre le Cancer (Comité de l'Ain), the Lyon Integrated Research Institute in Cancer (SIRIC LYriCAN INCa-DGOS-Inserm_12563), the Institut Convergence PLAsCAN (ANR-17-CONV-0002), the ERiCAN program of Fondation MSD-Avenir (Reference DS-2018-0015), the Institut National contre le Cancer (INCA-DGOS PRTK), the Société Française de Dermatologie (SFD), the association Melarnaud and Vaincre le Mélanome. MelBase is sponsored by the French National Cancer Institute (INCa).

**Corresponding author:**

Julie Caramel
Cancer Research Center of Lyon (CRCL)
« Cancer cell plasticity in melanoma » team
Centre Léon Bérard
Bâtiment Cheney D, 4th floor
28, rue Laënnec
69373 LYON Cedex 08, FRANCE
Tel: 33 (0) 426 556 705
Fax: 33 (0) 478 782 720
julie.caramel@lyon.unicancer.fr

**Competing interests.** The authors declare that no conflict of interest exists.

**Word count:** 6192

**Total number of figures:** 8

**Abstract (238 words)**

Cell plasticity sustains intra-tumor heterogeneity and treatment resistance in melanoma. Deciphering the transcriptional mechanisms governing reversible phenotypic transitions between proliferative/differentiated and invasive/stem-like states is required in order to design novel therapeutic strategies. EMT-inducing transcription factors, extensively known for their role in metastasis in carcinoma, display cell-type specific functions in melanoma, with a decreased ZEB2/ZEB1 expression ratio fostering adaptive resistance to targeted therapies. While ZEB1 direct target genes have been well characterized in carcinoma models, they remain unknown in melanoma. Here, we performed a genome-wide characterization of ZEB1 transcriptional targets, by combining ChIP-sequencing and RNA-sequencing, upon phenotype switching in melanoma models. We identified and validated ZEB1 binding peaks in the promoter of key lineage-specific genes related to melanoma cell identity. Comparative analyses with breast carcinoma cells demonstrated melanoma-specific ZEB1 binding, further supporting lineage specificity. Gain- or loss-of-function of ZEB1, combined with functional analyses, further demonstrated that ZEB1 negatively regulates proliferative/melanocytic programs and positively regulates both invasive and stem-like programs. We then developed single-cell spatial multiplexed analyses to characterize melanoma cell states with respect to ZEB1/ZEB2 expression in human melanoma samples. We characterized the intra-tumoral heterogeneity of ZEB1 and ZEB2 and further validated ZEB1 increased expression in invasive cells, but also in stem-like cells, highlighting its relevance *in vivo* in both populations. Overall, our results define ZEB1 as a major transcriptional regulator of cell states transitions and provide a better understanding of lineage-specific transcriptional programs sustaining intra-tumor heterogeneity in melanoma.

## 32-word statement of significance

We identify a ZEB1-driven, lineage-specific transcriptional program governing cell states transitions in melanoma, driving the emergence of invasive and stem-like states, and demonstrate its relevance in sustaining intra-tumor heterogeneity in human samples.

## Materials and Methods

### Human tumor samples

Melanoma tumor samples were obtained through the Biological Resource Center of the Lyon Sud Hospital (Hospices Civils de Lyon) and were used with the patient's written informed consent. This study was approved by a regional review board (Comité de Protection des Personnes Ile de France XI, Saint-Germain-en-Laye, France, number 12027) and is registered in ClinicalTrial.gov (MelBase, NCT02828202). 30 cutaneous melanoma patients were used for multi-immunofluorescence analyses. All melanoma biopsies were cutaneous, either primary melanoma or cutaneous metastases (Supplementary Table 1).

### Cell culture and treatments

The A375 human melanoma cell line was purchased from ATCC and cultured in DMEM complemented with 10% fetal bovine serum (FBS) (Cambrex) and 100 U/ml penicillin-streptomycin (Invitrogen). In order to authenticate the cell lines, the expected major genetic alterations were verified by NGS sequencing. The absence of Mycoplasma contamination was verified every 3 weeks with the MycoAlert detection kit (Lonza). Previously described patient-derived short-term cultures (<10), GLO and C-09.10, established from *BRAF*$^{V600}$ metastatic melanomas (21), were grown in RPMI complemented with 10% FBS and 100 U/ml penicillin-

streptomycin. TNFα (100 ng/mL) and TGFβ (20 ng/mL) (Peprotech) were replaced in the culture medium every 3 days. The BRAF inhibitor PLX4032/vemurafenib was purchased from Selleck Chemicals (Houston, TX, USA) and reconstituted in DMSO.

**Viral infections**

Generation of C-09.10 cells over-expressing ZEB1 using retroviral infection and HA-Zeb1 in a pBabe-puro vector was previously described (21). For *ZEB1* knock-out in A375 cells, human embryonic kidney 293T cells (4 x $10^6$) were transfected with lentiviral expression constructs (10 µg) in combination with GAG-POL (5 µg) and ENV expression vectors (10 µg). The constructs allowed the insertion, in an all-in-one manner, of the Cas9 nuclease and the guide RNA, scramble or targeting ZEB1, in a pLenti-Puro vector (pLenti-All-in-one-U6-sgRNA human Zeb1 (target1) or scramble -SFFV-Cas9 nuclease-2A-Puro) (Applied Biological Materials Inc., Richmond, Canada). The sequences of the sgRNA targeting ZEB1 are the following: human 5'-CACCTGAAGAGGACCAG-3' (F = forward), 5'-TCCTCTTCAGGTGCCTC-3' (R = reverse). The MITF promoter-GFP construct was purchased from GeneCopoeia (with a Hygromycin selection). Viral supernatants were collected 48 h post-transfection, filtered (0.45 µm membrane), and placed in contact with 2 x $10^6$ melanoma cells for 8 h in the presence of 8 µg/mL polybrene. Forty-eight h post-infection, cells were selected in the presence of puromycin (1 µg/mL) or hygromycin (500 µg/mL for GLO and 400 µg/mL for C-09.10) (Invitrogen).

**Immunoblot analyses**

Cells were washed twice with phosphate buffered saline (PBS) containing $CaCl_2$ and then lysed in a 100 mM NaCl, 1% NP40, 0.1% SDS, 50 mM Tris pH 8.0 RIPA buffer supplemented with a complete protease inhibitor cocktail (Roche, Mannheim, Germany) and phosphatase

inhibitors (Sigma-Aldrich). Loading was controlled using anti-GAPDH. Horseradish peroxidase-conjugated goat anti-rabbit polyclonal antibodies (Glostrup) were used as secondary antibodies. Western blot detections were conducted using the Luminol reagent (Santa Cruz). Western Blot Digital Imaging was performed with the ChemiDoc™ MP Imager (Bio-Rad).

| | Reference | Species | Dilution |
|---|---|---|---|
| Anti-ZEB1 | Sigma-Aldrich, HPA027524 (RRID:AB_1844977) | Rabbit | 1/500 |
| Anti-ZEB2 | Sigma-Aldrich, HPA003456 (RRID:AB_10603840) | Rabbit | 1/500 |
| Anti-MITF | Millipore, MAB3747 (RRID:AB_570596) | Mouse | 1/500 |
| Anti-NGFR | Cell signaling, 8238S (RRID:AB_10839265) | Rabbit | 1/1000 |
| Anti-AXL | R&D Systems Bio-Techne, AF154 (RRID:AB_354852) | Goat | 1/200 |
| Anti-SOX10 | Santa cruz, sc-365692 (RRID:AB_10844002) | Mouse | 1/500 |
| Anti-SOX9 | Genetex, GTX109661 | Rabbit | 1/500 |
| Anti-GAPDH | Sigma-Aldrich, Cat# ABS16 (RRID:AB_10806772) | Rabbit | 1/20000 |

## RT-Q-PCR

Total RNA was isolated using the RNeasy Kit (QIAGEN) and reverse-transcribed using a high cDNA capacity reverse transcription kit (Maxima First Strand cDNA synthesis Kit, Thermoscientific) following the manufacturer's instructions. Real-time PCR intron-spanning assays were designed using the ProbeFinder software (Roche). All reactions, including no-template controls and RT controls were performed in triplicate on a CFX96 (Bio-Rad) and were analyzed with the Bio-Rad CFX manager software. Human GAPDH was used for normalization.

| Gene | Sequence | | | |
|---|---|---|---|---|
| GAPDH | F | AGCCACATCGCTCAGACAC | R | GCCCAATACGACCAAATCC |
| ZEB1 | | AACTGCTGGGAGGATGACAC | | TCCTGCTTCATCTGCCTGA |
| ZEB2 | | AAGCCAGGGACAGATCAGC | | GCCACACTCTGTGCATTTGA |
| MITF-M | | CATTGTTATGCTGGAAATGCTAGA | | TGCTAAAGTGGTAGAAAGGTACTGC |
| NGFR | | ACAAGACCTCATAGCCAGCAC | | TGCAGCTGTTCCACCTCTTGA |
| AXL | | GGTGGCTGTGAAGACGATGA | | CTCAGATACTCCATGCCACT |
| SOX10 | | GGC-TCC-CCC-ATG-TCA-GAT | | CTG-TCT-TCG-GGG-TGG-TTG |
| SOX9 | | GTACCCGCACTTGCACAAC | | TCTCGCTCTCGTTCAGAAGTC |
| BIRC3 | | TCTGGGCAGCAGGTTTACAA | | CCCGAGATTAGACTAAGTCCCTT |
| ITGA2 | | AGACGTGCTCTTGGTAGGTG | | GCTGACCCAAAATGCCCTCT |
| EGFR | | AGCAGTCACTGGGGGACTT | | GGAGAGGAGAACTGCCAGAA |

## RNA-seq analyses

RNA libraries were prepared with the TrueSeq poly-A+ kit from Illumina and sequenced on the genomic platform of the CRCL, on an Illumina NovaSeq 6000 sequencing machine with a paired-end protocol (2x75bp, 32Mp reads). Raw sequencing reads were aligned on the human genome (GRCh38) with STAR (v2.7.8a), with the annotation of known genes from gencode v37. Gene expression was quantified using Salmon (1.4.0) and the annotation of protein-coding genes from gencode v37.

Bulk RNA-seq data of melanoma cell lines from Tsoi et al. (29) was retrieved from GEO, with accession number GSE80829. Single-cell RNAseq data of patient derived xenograft from Rambow et al. (15) were obtained from GEO with accession number GSE116237. Single-cell RNAseq data of melanoma cell lines from Wouters et al. (37) were analysed and visualized using Scope (https://scope.aertslab.org/#/Wouters_Human_Melanoma/).

## Chromatin immunoprecipitation and ChIP-sequencing analyses

The ChIP assay was carried out according to the protocol from the iDeal ChIP-Seq Kit for Transcription Factors (Diagenode). Briefly, cells from one 15-cm dish were cross-linked with 1% formaldehyde at RT for 10 min and quenched in 125 mM glycine for 5 min. Cross-linked chromatin was isolated and sonicated to generate DNA fragments averaging 200-500 bp in length by Bioruptor plus sonication device (Diagenode). Chromatin fragments were immunoprecipitated with antibodies directed against ZEB1 (1 µg, Genetex, GTX105278, RRID:AB_11162905), or IgG (1 µg, Bio-Rad, PRABP01, RRID:AB_321631) as negative control. Immunoprecipitated DNA was purified and dissolved into 25 µl of $H_2O$. To build the Illumina library, 5 ng of input and 30 pg of IP were used. Sequencing was performed on the CLB genomic platform, on an Illumina NextSeq machine with a paired-end protocol (2x75bp,

64Mp reads). To assess the efficacy of the ChIP before sequencing, MITF (positive control) was analyzed by qPCR. Primers were specified to amplify genomic DNA using the sequence from the peak (ChIPSeq data from MDAMB231, A375 or GLO cells). Relative promoter enrichment was normalized against chromatin inputs.

| Gene | Sequence | | | |
|---|---|---|---|---|
| ZEB2 | F | AATAGAGCAGGACCTCTCCCC | R | AGGTGTCCTTTGCTATCCAGC |
| MITF | | GGATTTCGAAGTCGGGGAGG | | CTGCTCTTCAGCGGTTGACT |
| NGFR | | TACGTCTCGGGGTGCAGA | | TGCGTAGCCAGAGCTGC |
| AXL | | CCGGGACTGTACTGTTTCTCC | | CCGTTCCCAGACAAGGTCAG |
| SOX10 | | AGACTCTAGGTGGGTGCGTC | | CCCACACCAAGAGACGGTTG |
| BIRC3 | | GGGGATTTGGGTGACGCATT | | ACAAGCCCAGTCTTTTCAAGC |
| ITGA2 | | CCCTTTCTCCACCCACTTAGG | | GGGCACTAGCCCTAAACCAC |
| EGFR | | GACAGGCCACCTCGTCG | | CCGGCTCTCCCGATCAATAC |

Two biological replicates from two independent experiments were performed for each ChIP-seq. DNA libraries were prepared with the Diagenode MicroPlex Library Preparation Kit v2, and sequenced on a NextSeq sequencing machine (paired-end protocol, 75bp, 80 M reads) on the genomic platform of the Centre Léon Bérard (CLB).

Public ZEB1 ChIP-seq data generated in MDA-MB-231 (23) were downloaded from EMBL-EBI (FASTQ files, accession number E-MTAB-8258). FOSL2 ChIP-seq data generated in SK-MEL-147 were retrieved from GEO with accession number GSE94488.

**Flow cytometry**

To analyze the expression of the NGFR/CD271 cell surface marker, cells 1 x $10^6$ cells per condition were incubated with an AlexaFluor647-conjugated anti-CD271 antibody (BD Pharmingen, RRID: AB_1645403) for 1 h in the dark before being counted on a BD LSRFortessa™ Flow Cytometer (BD Biosciences-IN). Data were analyzed using the FlowJo_V10 software.

**Transwell migration assay**

Falcon® Cell Culture Inserts for 24-well plates were placed into a 24-well plate, and 20% FBS RPMI was added into the well and 0.5% FBS RPMI was added into inserts. The plate was then incubated for 1 h for an initial equilibrium period. 200,000 GLO or 250,000 A375 cells were trypsinated and rinsed with 0.5% FBS RPMI medium. 100 µl 0.5% FBS RPMI containing 200,000 GLO cells was seeded into the insert, then 600 µl 20% FBS RPMI was added to the well. After 24 h incubation, cells inside the insert were removed carefully and the migrated cells on the membrane were fixed and colored using 4% PFA and Brilliant Blue, then rinsed with PBS. When inserts were completely dry, cells were viewed using phase-contrast microscopy. Photos were taken and analyzes by ZEISSZEN Microscope software. Migrated cells were counted in 3 different fields.

**Incucyte® Live Cell mortality measurement**

30,000 cells were seeded onto a 24-well plate and treated with TNFα+/-TGFβ. After 24 h, cell medium was renewed with indicated treatments, as well as PLX4032 and propidium iodide (Sigma-Aldrich®, 1/3000). The EssenBioScience IncuCyte Zoom Live-Cell Analysis System was used to measure and analyze real-time cell mortality every 2 h. Dead cells were marked with propidium iodide. Data were then converted into Excel in order to draw graphs.

**7-color immunofluorescence multiplex analyses**

3-µm tissue sections were cut from formalin-fixed paraffin-embedded human melanoma specimens. The sections underwent immunofluorescence staining using the OPAL™ technology (Akoya Biosciences) on a Leica Bond RX. A 7-color panel was designed. DAPI was used for nuclei detection.

| Antibody | Reference | Dilution | Staining localization |
|---|---|---|---|
| **ZEB1** | HPA02752 (RRID:AB_1844977) Sigma | 1/100 | Nuclear |
| **SOX10** | sc-365692 (RRID:AB_1084400) Santa Cruz | 1/1000 | Nuclear |
| **SOX9** | HPA001758 (RRID:AB_1080067) Sigma | 1/300 | Nuclear |
| **NGFR** | CS8238 (RRID:AB_10839265) Cell-signaling | 1/1500 | Membrane |
| **ZEB2** | HPA003456 (RRID:AB_10603840) Sigma | 1/300 | Nuclear |
| **MITF** | 284M-96 (RRID:AB_1516912) Sigma | 1/200 | Nuclear /cytoplasmic |

Sections were digitized with a Vectra Polaris scanner (Perkin Elmer, USA). Using the Inform software (Perkin Elmer), an autofluorescence treatment of images was carried out and tissue segmentation was performed to identify epidermis, stroma and tumor. Cell segmentation was then applied to analyze the expression of each marker in each cell. The matrix of phenotype containing the X- and Y- positions of each cell as well as the mean nuclear-, cytoplasmic- and membrane- intensities of each fluorescence staining was then further analyzed using the R software. Tumors were spatially reconstructed using the R plot() function.

For quantitative analyses, melanoma cells were classified following the expression level of each marker. The following cut-off values were defined.

| Opal | Marker | Low | Intermediate | High |
|---|---|---|---|---|
| 480 | SOX10 | 2 | | 5,6 |
| 520 | ZEB1 | 3,5 | 7,2 | 11 |
| 570 | MITF | 0,435 | 0,725 | 1,45 |
| 620 | NGFR | | | 2 |
| 690 | SOX9 | 1,18 | 2,54 | 4,4 |
| 780 | ZEB2 | 0,3 | 0,63 | 1,1 |

## Statistical analyses

To ensure adequate power and decreased estimation error, we performed multiple independent repeats and experiments were conducted at least in triplicate. Data are presented as mean ±s.d. or ± s.e.m as specified in the figure legends. Statistical analyses were performed using GraphPad Prism 8 software (GraphPad Software, Inc., San Diego, USA) or R software (v4.1.0) and plots were generated with *ggplot2* (v3.3.5). All statistical tests were two-tailed and p-values were corrected, when indicated, with the Benjamini-Hochberg method. Paired student's *t* tests were used to compare the means of two groups. To determine significant differences between two groups, student's *t* tests or Mann Whitney tests were used as indicated in the figure legends.

## Data availability

The data reported in this paper are deposited in the Gene Expression Omnibus (GEO) database under accession numbers GSE201614 (superseries): subseries ChiP-Seq (GSE201612); RNA-seq (GSE201613).

## Introduction

Cell plasticity contributes to intra-tumor heterogeneity and sustains tumor adaptation and treatment resistance (1). Cutaneous malignant melanoma is an aggressive form of skin cancer arising from melanocytes. Despite recent advances in targeted therapies and immunotherapies for the treatment of metastatic melanoma, nearly 60% of patients still develop resistance. A major mechanism of resistance to treatments relies on the ability of cancer cells to adapt to their environment and change phenotypes, i.e. to display cellular plasticity (2). One of these non-genetic adaptive mechanisms, the epithelial-mesenchymal transition (EMT), is a reversible trans-differentiation process finely regulated by a network of transcription factors (EMT-TFs) belonging to the SNAIL, TWIST and ZEB families (3). EMT-TFs are aberrantly

reactivated in many cancers (4–6), particularly in carcinomas, where they play an oncogenic role by fostering metastasis and endowing cells with stem-like features (7,8).

Although EMT cannot be formally defined in non-epithelial cancers, a related process of cellular plasticity contributes to intra-tumor heterogeneity (ITH) in melanoma and relies on reversible phenotypic transitions between proliferative/differentiated and invasive/stem-like states (9). Loss of MIcrophthalmia-associated Transcription Factor (MITF), the master regulator of melanocyte differentiation, induces a reprogramming towards an invasive and stem-like phenotype in melanoma cells (10–12). Gene expression analyses of tumors at the single-cell level refined this phenotype-switching model, by including the description of intermediate states and major molecular regulators (13–16). Reprogramming towards a Neural Crest Stem Cell-like (NCSC) phenotype was proposed as an adaptive response to targeted therapy, accounting for therapy resilience (17). However, a deeper understanding of cellular and molecular mechanisms underlying phenotypic adaptations and thus, the exceptional capacity of melanoma cells to develop resistance to current therapeutic strategies, is still needed.

We previously showed that a switch from ZEB2 to ZEB1 expression is a poor prognostic factor in melanoma (18,19). ZEB2 is expressed in normal melanocytes and its expression progressively decreases during transformation to melanoma, while ZEB1 expression increases. ZEB2 supports melanoma cell proliferation and differentiation by activating *MITF* expression (20). ZEB1, on the contrary, inhibits *MITF* expression, promotes transition to an invasive phenotype and resistance to targeted therapies (21). Though direct target genes of ZEB1 have been characterized in carcinoma models (22,23), they remain unknown in melanoma. Nonetheless, cell type-specific targets are particularly expected, given the antagonistic functions of ZEB1/ZEB2 in melanoma.

Herein, in order to characterize ZEB1 function and provide a comprehensive view of its transcriptional target genes in a genome-wide manner, we performed ChIP-sequencing combined with RNA-sequencing upon phenotype switching in melanoma cells. We define ZEB1 as a major transcriptional regulator of genes associated with phenotypic transitions in melanoma. Specific markers were validated as ZEB1 direct target genes, upon ZEB1 gain- or loss-of-function. Their relevance in human samples was further addressed through multiplexed spatial analyses. Intra-tumor heterogeneity of markers of melanoma cell states according to ZEB1 expression in human samples demonstrated co-expression of ZEB1 with both stem-like and invasive markers, highlighting the relevance of ZEB1 in these two sub-populations.

## Results:

### Modeling phenotype switching towards ZEB1$^{high}$/MITF$^{low}$ NCSC/invasive state *in vitro*

In order to study the role of endogenous ZEB1 during phenotypic transitions in melanoma cells, we used two patient-derived short-term cultures, established with a low number of passages after culture (GLO and C-09.10). These two short-term cultures display a ZEB1$^{low}$/MITF$^{high}$ proliferative phenotype. As previously described, C-09.10 cells are highly melanocytic, while GLO cells tend towards a transitory state, with intermediate MITF expression (21). To induce phenotype switching towards a ZEB1$^{high}$/MITF$^{low}$ state, cells were treated every 3 days, for up to 14 days, with the inflammatory cytokine TNFα, a known inducer of dedifferentiation in melanoma cells (24). As expected, TNFα treatment decreased proliferation, but no significant cell death was observed (data not shown). Treatment with TNFα induced a switch towards a ZEB1$^{high}$/MITF$^{low}$ state in GLO cells (Fig. 1A-B). ZEB1 protein expression increased, while ZEB2 expression decreased upon treatment (Fig. 1A). Drastic down-regulation of MITF expression was observed after treatment. Interestingly, the

expression of the NCSC marker NGFR (Nerve Growth Factor Receptor) (25,26) and of the receptor tyrosine kinase AXL (27) was increased. Analysis of SOX10 and SOX9 expression (28) (Fig. 1A) confirmed a progressive switch, towards a putative undifferentiated state, losing SOX10, in favor of SOX9, according to the four melanoma cell states *as per* the nomenclature proposed by *Tsoi et al.* (29) (melanocytic, transitory, neural-crest like NCL and undifferentiated). mRNA expression levels of these markers of melanoma cell states were consistently modified with the protein (Fig. 1B), except for *ZEB2* mRNA which was not modified, consistent with previous reports (20). We confirmed in the RNA-seq dataset from *Tsoi et al.* the progressive increase in *ZEB1* expression in the NCL and undifferentiated states, while *ZEB2* was strongly expressed in the melanocytic state and gradually decreased during dedifferentiation (Supp. Fig. 1A). Importantly, this switch was reversible, since the withdrawal of TNFα promoted the return to baseline expression levels (Supp. Fig. 1B).

In C-09.10 cells, TNFα was combined with TGFβ in order to ensure an efficient phenotype switching, evidenced by decreased MITF expression (Supp. Fig. 1C). Drastic up-regulation of ZEB1 expression was associated with progressive ZEB2 protein level down-regulation upon TNFα + TGFβ treatment (Supp. Fig. 2A-B). NGFR and AXL expression were also induced, however, the SOX10/SOX9 switch was not observed in this model.

Precise monitoring of intra-tumor heterogeneity during phenotype transitions over time was achieved by flow cytometry using stable cell lines established with a *MITF* promoter-GFP reporter construct and combined with NGFR membrane staining. As previously mentioned, GLO cells exhibit a transitory phenotype, with about half of the cell population harboring either a $MITF^{high}$ or a $MITF^{low}$ state. TNFα treatment decreased the proportion of the $MITF^{high}$ population and led to the emergence of a $MITF^{low}/NGFR^{high}$ phenotype (representing about 70% of the population at day 7), before a transition towards a $MITF^{low}/NGFR^{low}$ population occurred (representing 22% of the population at day 14) (Fig. 1C). Similarly, in C-09.10 cells,

FACS analyses of NGFR in a *MITF*-GFP reporter line, showed a decrease in the $MITF^{high}$ population and a transient increase in $MITF^{low}/NGFR^{int/high}$ cell population upon TNFα + TGFβ treatment (Supp. Fig. 2C).

Finally, we performed functional assays to validate the transition towards a more invasive state. Transwell migration assays validated that TNFα treatment progressively increased the migratory capacity of GLO cells (Fig. 1D). Consistent with their increased migratory capacity, the sensitivity of TNFα-treated GLO cells to the BRAF inhibitor (BRAFi) PLX4032 was also decreased compared to control cells, as assessed by Incucyte live-cell analysis (Fig. 1E). TNFα + TGFβ treated C-09.10 cells also exhibited increased resistance to BRAFi (Supp. Fig. 2D). These data confirmed the transition towards a more invasive and targeted-therapy resistant state.

In order to further characterize dysregulated pathways, we performed RNA-seq at day 7 and day 14 after TNFα +/- TGFβ treatment in GLO and C-09.10 cells. Pathway analyses of the 4531 differentially expressed (DE) genes at day 14 compared to untreated GLO cells ($p < 0.001$ & $|lFC| > 1$) (2490 up and 2041 down), confirmed a decrease in proliferation hallmarks, as well as an enrichment in TNFα signaling, inflammatory response, and EMT hallmarks (Fig. 1F & Supp. Fig. 3A, C). We next analyzed previously described proliferative and invasive melanoma signatures from *Hoek et al.* and *Verfaillie et al.* (30,31). Gene Set Enrichment Analysis (GSEA) confirmed a progressive switch from a proliferative/melanocytic (untreated), towards a more invasive state upon TNFα treatment (Fig. 1F-G & Supp. Fig. 3C). The NCSC (i.e. NCL) and undifferentiated state signatures from *Tsoi et al.* (29) were also activated at day 14, while the transitory state signature decreased in this model. RNA-seq analyses confirmed that C-09.10 cells display a more melanocytic phenotype than GLO cells, but similar pathways and signatures were consistently altered in this model (Fig. 1G and Supp. Fig. 3B, D-E). Computational inference of transcription factor (TF) activity, with the VIPER algorithm,

confirmed MITF and SOX10 TF decreased activity (Fig 1H & Supp. Fig. 3F). Moreover, the activity of the Activator Protein-1 (AP-1) complex members JUN and FOS, the major regulators of the mesenchymal state (32), was induced upon TNFα treatment in both GLO and C-09.10 cells, as well as that of the NF-κB subunits (RELA and NFKB1) (Fig 1H & Supp. Fig. 3F). Of note, ZEB1 and ZEB2 TF activity could not be reliably assessed based on DoRothEA pan-cancer database, because of melanoma cell-type specificities.

Overall, we developed two suitable *in vitro* models to study the direct transcriptional targets of endogenous ZEB1 during phenotypic transitions of melanoma cells towards ZEB1$^{high}$ NCSC-like and invasive states.

**Determination of ZEB1 direct target genes during phenotype switching**

In order to obtain a comprehensive view of endogenous ZEB1 direct target genes in a genome-wide manner, we performed chromatin immunoprecipitation coupled to deep sequencing (ChIP-seq) analyses with an anti-ZEB1 antibody, in untreated (ZEB1$^{low}$) and TNFα-treated (ZEB1$^{high}$) GLO cells at day 14, but also in the A375 melanoma cell line, which displays a ZEB1$^{high}$ NCSC-like expression pattern (MITF$^{low}$, NGFR$^{high}$, SOX10$^{+}$, SOX9$^{-}$) (Fig. 2). Consistent with increased ZEB1 expression, two-fold greater ZEB1 peaks were found in TNFα-treated GLO cells compared to untreated cells (Fig. 2A). 37% of ZEB1 peaks were conserved between ZEB1$^{low}$ (untreated) and ZEB1$^{high}$ (TNFα-treated) cells, while 63% were acquired upon TNFα-induced ZEB1 expression (Fig. 2B). Interestingly, 43% of ZEB1 peaks observed in TNFα-treated GLO cells were conserved in A375 cells (Fig. 2A-B). A large proportion of ZEB1 peaks (62% in TNFα-treated GLO cells) were found in promoter regions (-1000, +0bp), predominantly centered on the Transcription Start Site (Fig. 2C-D). Motif enrichment analyses of the top 1000 peaks in TNFα-treated GLO cells, when considering a 50 bp region centered on the ZEB1 peak, confirmed an enrichment in the ZEB1 binding motif,

which ranked first (Fig. 2E), sustaining the notion of a direct binding of ZEB1. When analysing a larger region of 200 bp centered on the ZEB1 peak, an enrichment in the AP-1 complex member transcription factor FOS binding motif was now evidenced (Supp. Fig. 4A). The clustering of the peak density of ZEB1 with publicly available ChIP-Seq data of FOSL2 (33) revealed a co-occupancy of FOSL2 at ZEB1 binding loci (Supp. Fig. 4B).

We initially focused on all genes presenting a ZEB1 binding peak in GLO cells after TNFα treatment (Fig. 2F). Pathway analyses on all these genes showed, aside from proliferation (E2F targets, G2M checkpoint) and inflammation (TNF, interferon signalling) hallmarks, a striking enrichment in melanoma signatures (Fig. 2F). Next, integration with RNA-seq data (TNFα differentially expressed genes, $p < 0.001$ and $|lFC| > 1$) allowed us to correlate binding of ZEB1 with transcriptional up- or down-regulation (Supp. Fig. 5A). Interestingly, a significant enrichment in the proportion of genes bound by ZEB1 was found, with 42% of dysregulated genes during phenotype switching exhibited a ZEB1 peak, 47% among down-regulated genes, and 38% among up-regulated genes (Supp. Fig. 5B). Pathway analyses on differentially expressed genes displaying a ZEB1 peak demonstrated that ZEB1 directly binds to down-regulated genes involved in proliferation hallmarks and to up-regulated genes involved in TNF signaling and invasion/EMT hallmarks (Fig. 2G). Highly significant enrichment in invasive, undifferentiated and NCSC melanoma signatures was unveiled among up-regulated genes presenting a ZEB1 binding peak. Importantly, ZEB1 was more frequently bound in baseline conditions, in untreated ZEB1$^{low}$ cells, to genes that are down-regulated upon phenotype switching, while it was more frequently recruited *de novo* to genes that are activated during the transition to the NCSC-like and invasive states (Fig. 2G).

A further analysis of melanoma phenotype signatures from *Hoek et al.* (31) demonstrated that ZEB1 binding peaks were present in 40% of genes of the proliferative signature, which are down-regulated upon phenotype switching (among which *MITF*, *PMEL*,

*CDH1*, *RAB38*, *ASAH1*, *TNFRSF14*) (Fig. 3A); 47% of invasive signature genes (which are activated upon phenotype switching) also displayed a ZEB1 binding peak (including *ZEB1* itself, *AXL*, *THBS1*, *BIRC3*, *ITGA2*, *ITGA3* and *EGFR*) (Fig. 3A). With respect to *Tsoi et al.* signatures, ZEB1 binding peaks were found in the promoter of 40% of genes of the melanocytic signature (including *CEACAM1* and *TSPAN10*), 35% of NCL signature genes (among which *TGFA*, *GLI2*, *NES*, *ANGPTL4*) and 33% of undifferentiated signature genes (including *EGFR* again, *SOX9*, *CITED2*, *KRT7*, *KRT18*, *KRT80*, *AJUBA*) (Fig. 3B). Only 17% of transitory signature genes displayed ZEB1 binding peaks (Fig. 3B). ZEB1 peaks were also identified in 41% and 32% of genes from the proliferative and invasive signatures from *Verfaillie et al.*, respectively (Supp. Fig. 5C). Importantly in the A375 cell line, the percentages of genes presenting a ZEB1 binding peak were largely similar to those described in GLO cells, more specifically in the invasive, NCL and undifferentiated signatures (Fig. 3B and Supp. Fig. 5C), highlighting the overall conservation in ZEB1 binding specificity in these two ZEB1$^{high}$ melanoma models.

Overall, combined RNA-seq and ChIP-seq analyses performed in two models, led to the identification of novel ZEB1 direct target genes, specific to the melanocytic lineage, including down-regulation of proliferative/melanocytic genes and up-regulation of NCSC and undifferentiated genes.

**ZEB1 directly regulates the expression of lineage-specific major markers of melanoma cell states**

We then focused on major markers of melanoma cell states: ZEB2, MITF, NGFR, AXL, SOX10 and SOX9. ZEB1 was already bound, in untreated GLO cells, to the promoters of *ZEB2*, *MITF* and *SOX10*, the expression of which is down-regulated upon phenotype switching towards a ZEB1$^{high}$ state (Fig. 4A). In contrast, a ZEB1 peak was acquired *de novo* during

phenotype switching in genes that are activated, such as *ZEB1* itself, *NGFR*, *AXL* and *SOX9*. Moreover, except for *SOX9*, which is not expressed in A375 cells, ZEB1 binding peaks were conserved in A375 cells, although not always at the same location (Fig. 4A).

Binding of ZEB1 to the sites defined by ChIP-seq was then validated by ChIP-qPCR in both GLO and C-09.10 models, upon phenotype switching towards a ZEB1$^{high}$ state and in A375 cells (Fig. 4B-C and Supp. Fig. 6A). Consistent with increased ZEB1 expression, an enrichment in the binding of this TF to the promoters of *ZEB2*, *MITF*, *NGFR*, and *SOX10* was observed in A375 cells, and in the GLO and C-09.10 models upon phenotype switching.

In order to reinforce the driving role of ZEB1 in the regulation of these genes, their expression was analyzed upon ZEB1 over-expression in C-09.10 and *ZEB1* knock-out in A375 cells (Fig. 5A-B). A pair of A375 *ZEB1* control (AS3) and knocked-out (AZ1) clones was analyzed, which did not show any defect in proliferation, albeit *ZEB1* knock-out in A375 cells was confirmed to decrease cell migration (Fig. 5C), further validating the key role of ZEB1 in this process. MITF and NGFR expression following ZEB1 dysregulation has previously been described (21). Here, we further witnessed that AXL is upregulated by ZEB1, following the same expression profile as NGFR. AXL expression decreased upon *ZEB1* knock-out in A375 cells. We further demonstrated that SOX10 expression decreased upon ZEB1 over-expression in C-09.10 although its expression was not further increased upon *ZEB1* knock-out in A375 cells. Inversely, SOX9 expression increased upon ZEB1 over-expression in C-09.10, and remained low upon *ZEB1* knock-out in A375 cells. Overall, our data sustain a model in which ZEB1 directly represses *MITF*, *SOX10*, and *ZEB2* and induces itself, *NGFR*, *AXL* and *SOX9*.

RNA-Seq analyses upon ZEB1 over-expression in C-09.10 further demonstrated the increase in EMT/invasion pathways (Fig. 5D). The most significantly enriched melanoma signatures among activated genes were the invasive and the NCSC (Fig. 5D-E). Interestingly, similarly to TNFα + TGFβ treatment, overexpression of ZEB1 was sufficient to induce

decreased activity of MITF TF, as well as increased activity of RELA and FOS/JUN (Fig 5F). Altogether, these results further support the conclusion that a major part of TNFα-mediated transition towards a more invasive/NCSC-like state is regulated by ZEB1.

Interestingly, beyond well-described phenotypic markers from Figure 4, ZEB1 binding peaks were found in other major markers of melanoma cell identity, namely *BIRC3*, *ITGA2* and *EGFR*, which are up-regulated upon phenotype switching towards the ZEB1$^{high}$ state as confirmed by RT-qPCR (Supp. Fig. 6B-C). ZEB1 binding on the promoters of these genes could also be confirmed by ChIP-qPCR (Supp. Fig. 6D).

Finally, in order to analyze the lineage specificity of ZEB1 binding compared to carcinoma models, we performed a comparative analysis with a previously published ZEB1 ChIP-seq dataset performed in the MDA-MB-231 breast cancer cell line (23). Interestingly, while some ZEB1 peaks were conserved in MDA-MB-231, peaks in *SOX10* and *NGFR* were only found in melanoma cells (Fig. 4A). Other genes involved in oncogenesis bore melanoma-specific ZEB1 binding sites which were either lost in MDA-MB-231 cells, such as for the WNT regulators *TLE4* (Groucho) (which is down-regulated upon ZEB1 over-expression) and *SFRP1* (which is up-regulated upon ZEB1 over-expression), or had an altered position in the breast cancer cell line, such as *FOXC2* for example (34) (Supp. Fig. 6E). Furthermore, several melanocyte differentiation-related genes, namely the anti-apoptotic gene *BCL2*, a known MITF target (35), and *BLOC1S5*, the mutation of which is associated with defects in pigmentation (36), also displayed melanoma-specific ZEB1 binding peaks, further supporting lineage specificity of ZEB1 binding in melanoma cells compared to carcinoma cells.

**Single-cell and spatial analyses of ZEB1 intra-tumor heterogeneity in melanoma patient samples**

To further investigate the correlation between the expression of ZEB1 and markers of melanoma cell states at the single-cell level, we first used publicly available single-cell RNA-seq datasets. In the panel of 10 melanoma cell lines from *Wouters et al.* (37), including the A375 cell line, ZEB1 was preferentially expressed in mesenchymal-like cells, while ZEB2 was found in melanocyte-like cells (Fig. 6A). We observed *ZEB1* co-expression at the single-cell level with markers of the NCSC or the undifferentiated phenotype, *NGFR* and *SOX9*, respectively, and confirmed its antagonistic expression pattern with *MITF* and *SOX10*, markers of the melanocytic/proliferative phenotype. In addition, in the scRNA-seq dataset of melanoma PDX tumors from *Rambow et al.* (15), *ZEB1* expression was significantly increased in the NCSC and the invasive populations, compared to the pigmented state (Fig. 6B). Importantly, *ZEB1* is part of the top 200 genes enriched in the NCSC signature. *ZEB1* expression was also found in intermediate states, including the SMC (Starved Melanoma Cell) phenotype (Fig. 6B).

In order to further investigate ZEB1 co-expression or antagonistic expression with markers of melanoma cell states in patient samples, we performed spatial multi-immunofluorescence analyses (7 colors, OPAL, Perkin-Elmer) in a cohort of 30 cutaneous melanomas, including 12 previously annotated ZEB1$^{high}$ melanomas (Supplementary Table 1). We analyzed at single-cell resolution the protein expression levels of ZEB1, ZEB2, MITF, NGFR, SOX10 and SOX9 to precisely define the frequency and spatial organization of the different phenotypes (Fig. 7A). This technique enables the specific quantification of the level of expression of markers of melanoma cell state in ZEB1-expressing melanoma cells, and excludes other cells from the microenvironment (38).

Spatial reconstitution of the intensity of each marker at whole tumor level, revealed differential patterns of expression (Fig. 7B-D). Thin primary melanomas (such as Patient #A, Breslow = 0.8 mm) (Fig. 7A) or thick primitive melanomas (such as Patient #C, Breslow = 16 mm) (Fig. 7B) displayed a proliferative/differentiated ZEB2$^{+}$ MITF$^{+}$ SOX10$^{+}$ phenotype with

no or low ZEB1, SOX9 and NGFR expression (Fig. 7A-B). A gain in ZEB1 expression could be observed not only at the invasive front of primary melanomas, but also in the bulk, either in specific clones (as in Patient #D) (Fig. 7C) or in the whole tumor (as in Patient #B) (Fig. 7D). As shown in previous cohorts by immunohistochemistry (18,21), antagonistic expression patterns of ZEB1 and ZEB2, as well as ZEB1 and MITF were confirmed at the intra-tumoral level by immunofluorescence (Fig. 7A, C-D).

We next analyzed SOX10 intra-tumor heterogeneity in these ZEB1$^{high}$ tumors and evidenced cell populations with decreased SOX10 intensity. As illustrated in the Patient #D tumor, which bore the presence of a well-defined ZEB1$^{high}$ clone, increased ZEB1 expression was not only associated with low ZEB2 and MITF expression, but also with decreased SOX10 levels (Fig. 7C and 8A). Quantitative analyses of SOX10 intensity according to ZEB1 expression level (high, intermediate, low and negative) confirmed a significant decrease in SOX10 levels when ZEB1 expression increases in melanoma cells (Fig. 8B).

We then investigated a putative gain in the expression of NCSC and dedifferentiation markers, NGFR and SOX9, in tumors presenting a high ZEB1 expression. NGFR expression was observed in scarce sub-populations of cells. Interestingly, the ZEB1$^{high}$ clone from Patient #D case displayed NGFR positivity (Fig. 7C and 8C), and NGFR levels were significantly higher in ZEB1$^{high}$ melanoma cells (Fig. 8D).

SOX9 expression was only detected in a limited number of tumors, as exemplified by the ZEB1$^{high}$ Patient #B tumor which displayed high SOX9 levels (Fig. 7D and 8E). The antagonistic expression of SOX10 and SOX9 could clearly be evidenced at the single-cell level (Fig. 7A). Moreover, SOX9 levels were correlated with ZEB1 expression (Fig. 8F). Interestingly, only a few cells displayed triple positivity for ZEB1, NGFR and SOX9 (Fig. 8C).

Overall, single-cell and spatial characterization of melanoma intra-tumor heterogeneity demonstrate that increased ZEB1 expression is correlated with decreased MITF and SOX10

levels and increased NGFR or SOX9 expression, thus highlighting the importance of ZEB1 *in vivo* in both the NCSC and undifferentiated cell populations.

## Discussion

Our study reports a genome-wide characterization of the transcriptional functions of ZEB1 in melanoma, providing a better understanding of the molecular mechanisms underlying phenotype plasticity and intra-tumor heterogeneity in melanoma. We identified and validated the direct binding of the ZEB1 transcription factor to the promoter of genes specific to the melanocytic lineage or driving melanoma cell identity. Gain- or loss-of-function of ZEB1, combined with function analyses, further demonstrates that ZEB1 negatively regulates proliferative-melanocytic programs and up-regulates invasive/stem-like programs.

Overall, this study defines ZEB1 as a major regulator of melanoma cell identity and phenotype switching. Although initially described as a transcriptional repressor, our data confirm previous ChIP-seq analyses in carcinoma models (23) showing the capacity of ZEB1 to mediate both transcriptional activation and repression in similar proportions. Interestingly, at the basal level, ZEB1 mostly represses the expression of melanocytic genes, while increased ZEB1 expression upon phenotype switching, is associated with *de novo* binding, driving the up-regulation of invasive and NCSC genes. We propose a model in which ZEB1 may directly repress *MITF*, *SOX10*, and *ZEB2*, and in the meantime induce itself, *NGFR*, *AXL* and SOX9. Although ZEB1 binding peaks are observed, ZEB1 may not increase NCSC and undifferentiated markers in the same cells, nor at the same time. This is consistent with models proposed in carcinoma, where ZEB1 may promote stemness features (partial EMT state associated with tumor initiation) but not necessarily invasive/EMT features, these two features being uncoupled. Overall, ZEB1 may not be associated with the acquisition of a given cell state but may regulate reversible cell state transitions in a dynamic manner.

Importantly, even if some ZEB1 target genes are shared between melanoma and breast cancer cell lines (23), such as *CDH1* and other EMT genes, our study reveals cell type-specific effects of ZEB1, through the regulation of melanocytic lineage-specific genes. ZEB1 notably binds to the promoter of *ZEB2* and represses its expression in melanoma cells, while these two factors are co-expressed in mesenchymal cells. In this respect, a ZEB1 peak was observed in the *ZEB2* gene in MDA-MB-231 cells, but at a different location.

ZEB1 not only represses MITF expression and subsequently the MITF-transcriptional program, but also directly regulates known MITF targets. Previous MITF ChIP-seq analyses demonstrated that MITF directly and positively regulates genes involved in DNA replication, repair and mitosis, while repressing genes involved in melanoma invasion (39). ZEB1 and MITF may thus bind to the same genes but with different consequences.

AP-1 motif was found enriched at ZEB1 binding sites and the AP-1 subunit FOSL2 was shown to co-occupy similar loci with ZEB1, suggesting a cooperation of ZEB1 with AP-1 in melanoma. Furthermore, the TF activity of both JUN and FOS was enriched upon ZEB1 activation, suggesting a positive feedback loop on AP-1 activity. While YAP and AP1 were evidenced as the main TFs cooperating with ZEB1 in breast cancer cells (23), we observed in second position after the ZEB1 motif, an enrichment in the binding motif of a Zinc finger TF, called ZBTB33 (zinc finger and BTB domain containing 33, or Kaiso) (Fig. 2E), which was previously shown to promote EMT in prostate cancer (40). These observations further suggest cell-type specificities in the TF network cooperating with ZEB1. The precise characterization of ZEB1 cofactors would be required in order to better comprehend the complex role of ZEB1 during gene regulation in a context and cell type-specific manner.

Importantly, our quantitative spatial analyses at the single-cell resolution of markers of melanoma cell states in human samples provided further validation of the co-expression of ZEB1 with NCSC (NGFR) or undifferentiated (SOX9) markers and its inverse correlation with

the melanocytic markers MITF and SOX10. Although NGFR and SOX9 are not sufficient to define the NCSC and undifferentiated states respectively, ZEB1 expression may be found in these two subpopulations of cells. Importantly, ZEB1 is not only expressed in the invasive front but also in the bulk, where it may sustain stem-like features and tumor-initiating properties. SOX10 intra-tumor heterogeneity in melanoma samples was consistent with recent reports (41). However, only a few samples displayed a significant expression of NGFR or SOX9 and a strong inter-patient variability was observed among the 30 samples analyzed, leading to much more complex patterns of intra-tumor heterogeneity than in *in vitro* conditions.

TNFα and TGFβ mimic only part of the signals emanating from the tumor microenvironment. Indeed, we recently highlighted the major crosstalk existing between melanoma cells and their immune microenvironment (38,42) and recent work from the Marine lab highlighted the major role of endothelial cells in promoting a mesenchymal state (43). ZEB1 and other melanoma markers of intra-tumor heterogeneity may thus significantly be modified by the tumor microenvironment in specific niches that will deserve further characterization. Moreover, if we focused on markers of melanocyte cell identity, this ChIP-seq approach also revealed additional targets related to inflammatory or interferon responses, consistent with the pleiotropic roles of ZEB1, that extend beyond invasion, including immune escape (38).

Hence, this study provides important insights into the way ZEB1 orchestrates gene expression, with a precise combination of both down-regulation and up-regulation of key genes of melanoma cell state, which in turn mediate reversible phenotypic plasticity, known to foster the acquisition of resistance to treatment in melanoma. Although targeting ZEB1 remains challenging, this work highlights new candidates/pathways that could represent interesting targets to dampen melanoma cell plasticity as a strategy to overcome treatment resistance.

**Acknowledgments**

The authors would like to thank Brigitte Manship for critical reading as well as Irwin Davidson lab for helpful discussions. YT was supported by a fellowship from Ligue Nationale contre le Cancer and SD by a fellowship from the Association pour la Recherche contre le Cancer (ARC).

## Author contributions

YT and SDu designed, performed, analyzed experiments and prepared figures. MG, LB and FB performed and analyzed experiments. RP and EC performed ChIP-Seq and RNA-Seq bioinformatics analyses. VB, FD and MP contributed to multi-IF analyses and spatial reconstitution. SDa and AE provided human samples and clinical data. JC conceived and supervised the whole project and wrote the manuscript.

## References

1. Marine JC, Dawson SJ, Dawson MA. Non-genetic mechanisms of therapeutic resistance in cancer. Vol. 20, Nature Reviews Cancer. Nature Research; 2020. p. 743–56.
2. Arozarena I, Wellbrock C. Phenotype plasticity as enabler of melanoma progression and therapy resistance. Nat Rev Cancer. 2019;19(7):377–91.
3. Nieto MA, Huang RY, Jackson RA, Thiery JP. Emt: 2016. Cell. 2016;166(1):21–45.
4. Pastushenko I, Blanpain C. EMT Transition States during Tumor Progression and Metastasis. Vol. 29, Trends in Cell Biology. Elsevier Ltd; 2019. p. 212–26.
5. Brabletz S, Brabletz T. The ZEB/miR-200 feedback loop--a motor of cellular plasticity in development and cancer? EMBO Rep. 2010;11(9):670–7.
6. Tam WL, Weinberg RA. The epigenetics of epithelial-mesenchymal plasticity in cancer. Nat Med. 2013;11:1438–49.
7. Caramel J, Ligier M, Puisieux A. Pleiotropic roles for ZEB1 in cancer. Vol. 78, Cancer Research. 2018. p. 30–5.
8. Puisieux A, Brabletz T, Caramel J. Oncogenic roles of EMT-inducing transcription factors. Nat Cell Biol. 2014;16(6):488–94.
9. Hoek KS, Eichhoff OM, Schlegel NC, Döbbeling U, Kobert N, Schaerer L, et al. In vivo switching of human melanoma cells between proliferative and invasive states. Cancer Res. 2008;68(3):650–6.
10. Rambow F, Marine JC, Goding CR. Melanoma plasticity and phenotypic diversity: Therapeutic barriers and opportunities. Genes Dev. 2019;33(19–20):1295–318.
11. Goding CR, Arnheiter H. MITF — the first 25 years. 2019;1–25.
12. Cheli Y, Guiliano S, Botton T, Rocchi S, Hofman V, Hofman P, et al. Mitf is the key molecular switch between mouse or human melanoma initiating cells and their differentiated progeny. Oncogene. 2011;30(20):2307–18.
13. Ennen M, Keime C, Gambi G, Kieny A, Coassolo S, Thibault-carpentier C, et al. MITF-high and MITF-low cells and a novel subpopulation expressing genes of both cell states

contribute to intra and inter-tumoral heterogeneity of primary melanoma. Clinical cancer research. 2017;23(22):7097–107.
14. Jerby-Arnon L, Shah P, Cuoco MS, Rodman C, Su M ju, Melms JC, et al. A Cancer Cell Program Promotes T Cell Exclusion and Resistance to Checkpoint Blockade. Cell. 2018;175:984–97.
15. Rambow F, Rogiers A, Marin-bejar O, Aibar S, Femel J, Dewaele M. Toward Minimal Residual Disease-Directed Therapy in Melanoma Toward Minimal Residual Disease-Directed Therapy in Melanoma. Cell. 2018;1–13.
16. Tirosh I, Izar B, Prakadan SM, Wadsworth MH, Treacy D, Trombetta JJ, et al. Dissecting the multicellular ecosystem of metastatic melanoma by single-cell RNA-seq. Science 2016;352(6282):189–96.
17. Diener J, Sommer L. Reemergence of neural crest stem cell-like states in melanoma during disease progression and treatment. Vol. 10, Stem Cells Translational Medicine. John Wiley and Sons Ltd; 2021. p. 522–33.
18. Caramel J, Papadogeorgakis E, Hill L, Browne GJ, Richard G, Wierinckx A, et al. A Switch in the Expression of Embryonic EMT-Inducers Drives the Development of Malignant Melanoma. Cancer Cell. 2013;24(4):466–80.
19. Tang Y, Durand S, Dalle S, Caramel J. EMT-Inducing Transcription Factors, Drivers of Melanoma Phenotype Switching, and Resistance to Treatment. Cancers (Basel). 2020;12:2154.
20. Vandamme N, Denecker G, Bruneel K, Blancke G, Akay Ö, Taminau J, et al. The EMT transcription factor ZEB2 promotes proliferation of primary and metastatic melanoma while suppressing an invasive, mesenchymal-like phenotype. Cancer Research. 2020.
21. Richard G, Dalle S, Monet MA, Ligier M, Boespflug A, Pommier RM, et al. ZEB1-mediated melanoma cell plasticity enhances resistance to MAPK inhibitors. EMBO Mol Med. 2016;8(10):1143–61.
22. Katsura A, Tamura Y, Hokari S, Harada M, Morikawa M, Sakurai T, et al. ZEB1-regulated inflammatory phenotype in breast cancer cells. Mol Oncol. 2017 Sep;11(9):1241–62.
23. Feldker N, Ferrazzi F, Schuhwerk H, Widholz SA, Guenther K, Frisch I, et al. Genome-wide cooperation of EMT transcription factor ZEB 1 with YAP and AP -1 in breast cancer. EMBO J. 2020;39(17):1–21.
24. Riesenberg S, Groetchen A, Siddaway R, Bald T, Reinhardt J, Smorra D, et al. MITF and c-Jun antagonism interconnects melanoma dedifferentiation with pro-inflammatory cytokine responsiveness and myeloid cell recruitment. Nat Commun. 2015;6:8755.
25. Restivo G, Diener J, Cheng PF, Kiowski G, Bonalli M, Biedermann T, et al. Low Neurotrophin receptor CD271 regulates phenotype switching in Melanoma. Nat Commun. 2017;8(1988):1–16.
26. Boshuizen J, Vredevoogd DW, Krijgsman O, Ligtenberg MA, Blankenstein S, de Bruijn B, et al. Reversal of pre-existing NGFR-driven tumor and immune therapy resistance. Nat Commun. 2020;11(1):1–13.
27. Müller J, Krijgsman O, Tsoi J, Robert L, Hugo W, Song C, et al. Low MITF/AXL ratio predicts early resistance to multiple targeted drugs in melanoma. Nat Commun. 2014;5(5712):1–15.
28. Shakhova O, Cheng P, Mishra PJ, Zingg D, Schaefer SM, Debbache J, et al. Antagonistic Cross-Regulation between Sox9 and Sox10 Controls an Anti-tumorigenic Program in Melanoma. PLoS Genet. 2015;11(1):1–21.
29. Tsoi J, Robert L, Paraiso K, Galvan C, Sheu KM, Lay J, et al. Multi-stage Differentiation Defines Melanoma Subtypes with Differential Vulnerability to Drug-Induced Iron-Dependent Oxidative Stress. Cancer Cell. 2018 May;33(5):890-904.e5.

30. Verfaillie A, Imrichova H, Atak ZK, Dewaele M, Rambow F, Hulselmans G, et al. Decoding the regulatory landscape of melanoma reveals TEADS as regulators of the invasive cell state. Nat Commun. 2015;6(6683):1–16.
31. Hoek KS, Schlegel NC, Sucker A, Ugurel S, Weber BL, Katherine L, et al. Metastatic potential of melanomas defined by specific gene expression profiles with no BRAF signature. Pigment Cell Melanoma Res. 2006;19:290–302.
32. Mauduit D, Taskiran II, Minnoye L, de Waegeneer M, Christiaens V, Hulselmans G, et al. Analysis of long and short enhancers in melanoma cell states.
33. Fontanals-Cirera B, Hasson D, Vardabasso C, di Micco R, Agrawal P, Chowdhury A, et al. Harnessing BET Inhibitor Sensitivity Reveals AMIGO2 as a Melanoma Survival Gene. Mol Cell. 2017 Nov 16;68(4):731-744.e9.
34. Hargadon KM, Gyorffy B, Strong EW, Tarnai BD, Jefferson CT, Bushhouse DZ, et al. The FOXC2 transcription factor promotes melanoma outgrowth and regulates expression of genes associated with drug resistance and interferon responsiveness. Cancer Genomics Proteomics. 2019;16(6):491–503.
35. McGill GG, Horstmann M, Widlund HR, Du J, Motyckova G, Nishimura EK, et al. Bcl2 Regulation by the Melanocyte Master Regulator Mitf Modulates Lineage Survival and Melanoma Cell Viability. Vol. 109, Cell. 2002.
36. Pennamen P, Le L, Tingaud-Sequeira A, Fiore M, Bauters A, Van N, et al. BLOC1S5 pathogenic variants cause a new type of Hermansky-Pudlak syndrome. Genetics in Medicine. 2020;22:1613–22.
37. Wouters J, Kalender-Atak Z, Minnoye L, Spanier KI, de Waegeneer M, Bravo González-Blas C, et al. Robust gene expression programs underlie recurrent cell states and phenotype switching in melanoma. Nat Cell Biol. 2020;22(8):986–98.
38. Plaschka M, Benboubker V, Grimont M, Berthet J, Tonon L, Lopez J, et al. ZEB1 transcription factor promotes immune escape in melanoma. J Immunother Cancer. 2022 Mar 14;10(3):e003484.
39. Laurette P, Strub T, Koludrovic D, Keime C, Le Gras S, Seberg H, et al. Transcription factor MITF and remodeller BRG1 define chromatin organisation at regulatory elements in melanoma cells. Elife. 2015;2015(4):1–40.
40. Abisoye-Ogunniyan A, Lin H, Ghebremedhin A, Salam A bin, Karanam B, Theodore S, et al. Transcriptional repressor Kaiso promotes epithelial to mesenchymal transition and metastasis in prostate cancer through direct regulation of miR-200c. Cancer Lett. 2018 Sep 1;431:1–10.
41. Capparelli C, Purwin TJ, Glasheen M, Caksa S, Tiago M, Wilski N, et al. Targeting SOX10-deficient cells to reduce the dormant-invasive phenotype state in melanoma. Nat Commun. 2022 Dec 16;13(1):1381.
42. Benboubker V, Boivin F, Dalle S, Caramel J. Cancer Cell Phenotype Plasticity as a Driver of Immune Escape in Melanoma. Front Immunol. 2022 Mar 29;13.
43. Karras P, Bordeu I, Pozniak J, Nowosad A, Pazzi C, van Raemdonck N, et al. A cellular hierarchy in melanoma uncouples growth and metastasis. Nature. 2022 Oct 6;610(7930):190–8.

Figure 1

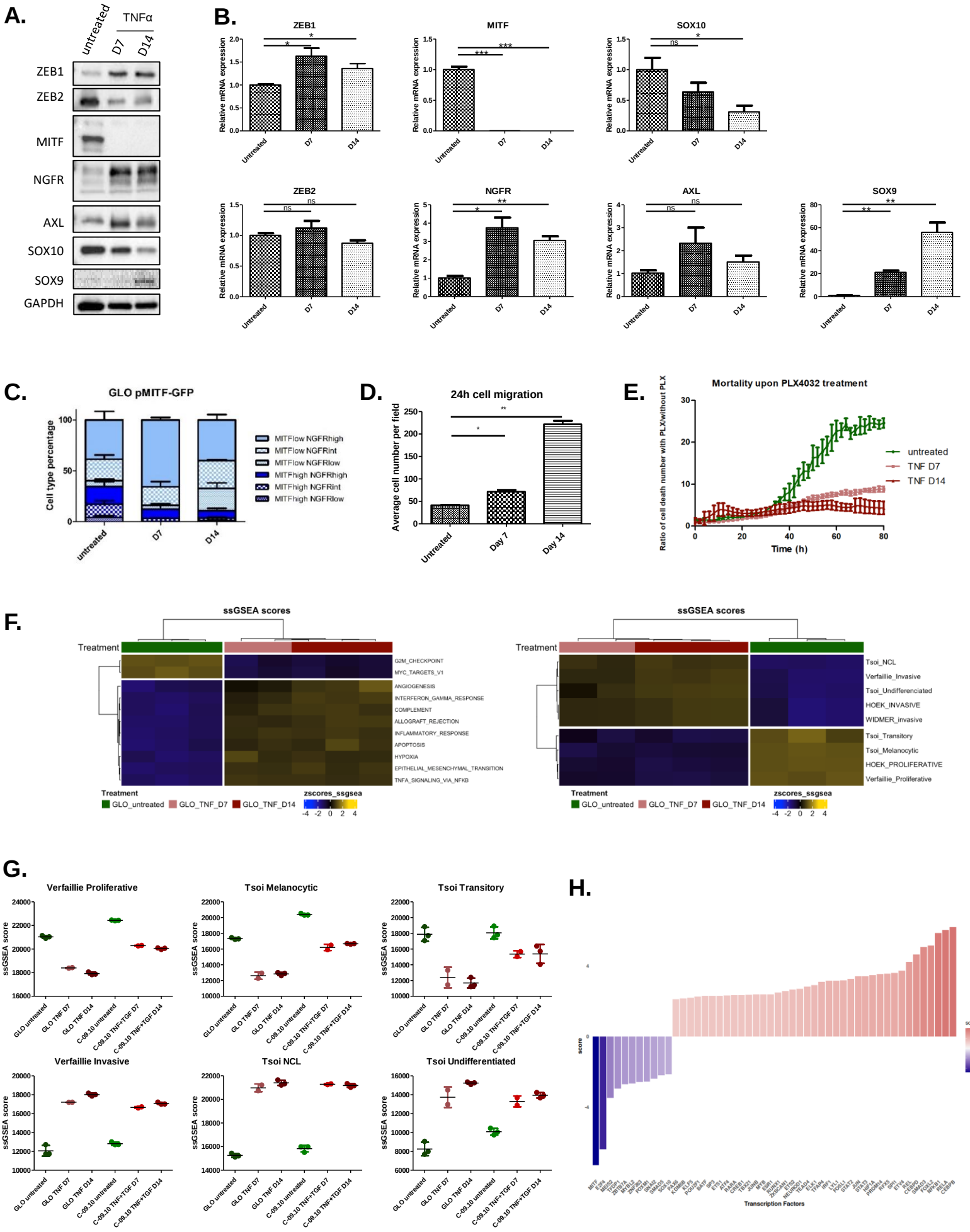
A.
untreated
TNFα
D7
D14
ZEB1
ZEB2
MITF
NGFR
AXL
SOX10
SOX9
GAPDH
B.
ZEB1
MITF
SOX10
ZEB2
NGFR
AXL
SOX9
Relative mRNA expression
Untreated
D7
D14
C.
GLO pMITF-GFP
Cell type percentage
MITFlow NGFRhigh
MITFlow NGFRint
MITFlow NGFRlow
MITFhigh NGFRhigh
MITFhigh NGFRint
MITFhigh NGFRlow
D.
24h cell migration
Average cell number per field
Untreated
Day 7
Day 14
E.
Mortality upon PLX4032 treatment
Ratio of cell death number with PLX/without PLX
Time (h)
untreated
TNF D7
TNF D14
F.
ssGSEA scores
Treatment
G2M_CHECKPOINT
MYC_TARGETS_V1
ANGIOGENESIS
INTERFERON_GAMMA_RESPONSE
COMPLEMENT
ALLOGRAFT_REJECTION
INFLAMMATORY_RESPONSE
APOPTOSIS
HYPOXIA
EPITHELIAL_MESENCHYMAL_TRANSITION
TNFA_SIGNALING_VIA_NFKB
GLO_untreated
GLO_TNF_D7
GLO_TNF_D14
zscores_ssgsea
Tsoi_NCL
Verfaillie_Invasive
Tsoi_Undifferenciated
HOEK_INVASIVE
WIDMER_invasive
Tsoi_Transitory
Tsoi_Melanocytic
HOEK_PROLIFERATIVE
Verfaillie_Proliferative
G.
Verfaillie Proliferative
Tsoi Melanocytic
Tsoi Transitory
Verfaillie Invasive
Tsoi NCL
Tsoi Undifferentiated
ssGSEA score
GLO untreated
GLO TNF D7
GLO TNF D14
C-09.10 untreated
C-09.10 TNF+TGF D7
C-09.10 TNF+TGF D14
H.
score
Transcription Factors

**Figure 1. Modeling phenotype switching towards ZEB1$^{high}$/MITF$^{low}$ neural crest stem cell /invasive state *in vitro***

Western blot **(A)** and RT-qPCR **(B)** analyses of ZEB1, ZEB2, MITF, NGFR, AXL, SOX10 and SOX9 expression after 7 (D7) and 14 (D14) days of TNFα (100 ng/mL) treatment in GLO cells. GAPDH was used as loading control. Histograms represent quantitative analyses of relative expression (n = 4 independent experiments).

**C.** Longitudinal intra-tumor heterogeneity characterization of MITF and NGFR expression by flow cytometry in GLO pMITF-GFP cells, upon TNFα treatment during 7 (D7) or 14 (D14) days. NGFR was marked by anti-NGFR antibody coupled with APC. The proportion of cells with MITF high, intermediate or low and with NGFR high, intermediate or low statuses is indicated.

**D.** Transwell migration assays in GLO cells upon TNFα treatment after 7 (D7) or 14 (D14) days. Cells were fixed after 24 h, the number of migrating cells is plotted (n = 3).

**E.** Incucyte assay showing the relative increase in cell death upon PLX4032 (500 nM) treatment over time, in cells previously treated with TNFα for 7 or 14 days.

**F.** RNA-seq analyses of GLO cells after 7 (D7) or 14 days (D14) of TNFα treatment. Heatmap of ssGSEA scores of the most relevant hallmarks and of melanoma states signatures from Hoek, Tsoi, Verfaillie and Widmer. Clustering Ward.D2 / distance: Euclidean.

**G.** Scatter plot of the melanoma signatures ssGSEA scores (Tsoi and Verfaillie) in cells treated for 7 (D7) or 14 days (D14) with TNFα (GLO) or TNFα+TGFβ (C-09.10).

**H.** Inference of transcription factors (TF) activity in gene expression data using VIPER algorithm. Barplot of DoRothEA TF Normalized Enrichment Score (NES) comparing untreated versus TNF treated (D14) GLO cells.

Data are shown as the mean ± SEM. P values were determined by a two-tailed paired student *t* test **(B, D)**. Differences were considered statistically significant at $^{*}P \leq 0.05$, $^{**}P < 0.01$ and $^{***}P < 0.001$. ns (non-significant) means $P > 0.05$.

Figure 2

**A.**

| | Peak number | Mean size bp |
|---|---|---|
| **GLO_untreated** | 5195 | 542.76 |
| **GLO_TNF_D14** | 11779 | 580.26 |
| **A375_AS3** | 9861 | 538.50 |

**B.**

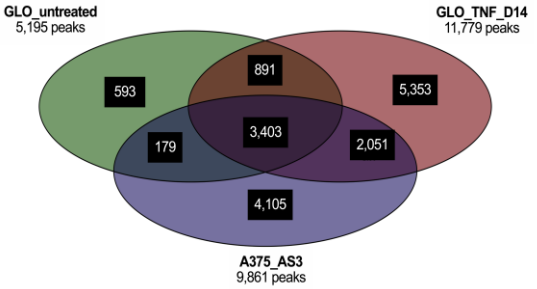


**C.**

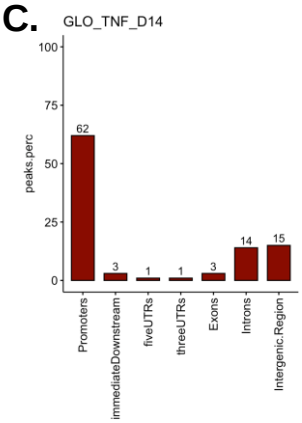


**D.**

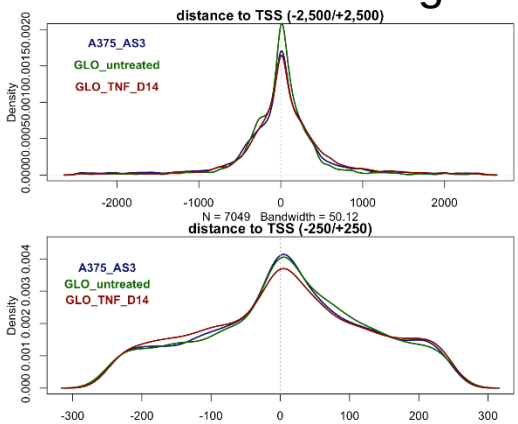


**E.**

| Rank | Motif | P-value | % of targets | % of background | Corresponding transcription factor |
|---|---|---|---|---|---|
| 1 |  | $1^{e}$-122 | 41.50% | 11.89% | ZEB1 |
| 2 |  | $1^{e}$-62 | 11.70% | 1.56% | ZBTB33 |
| 3 |  | $1^{e}$-27 | 3.70% | 0.29% | ATF4 |

**F.**

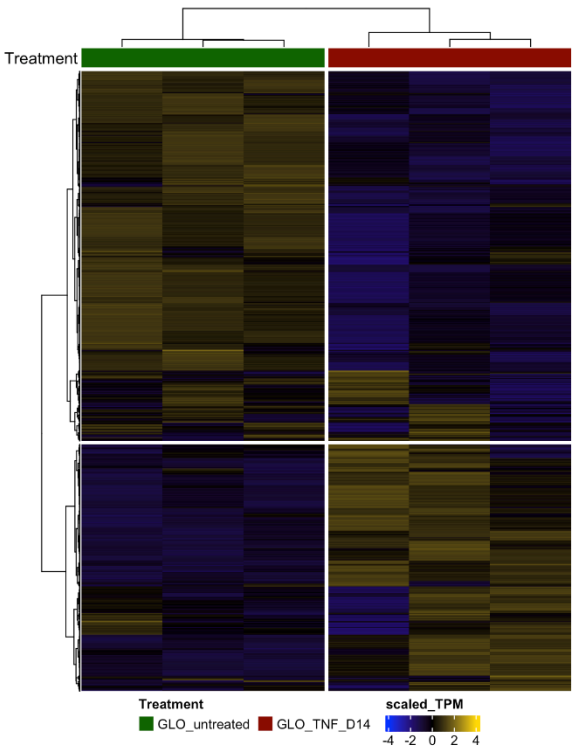


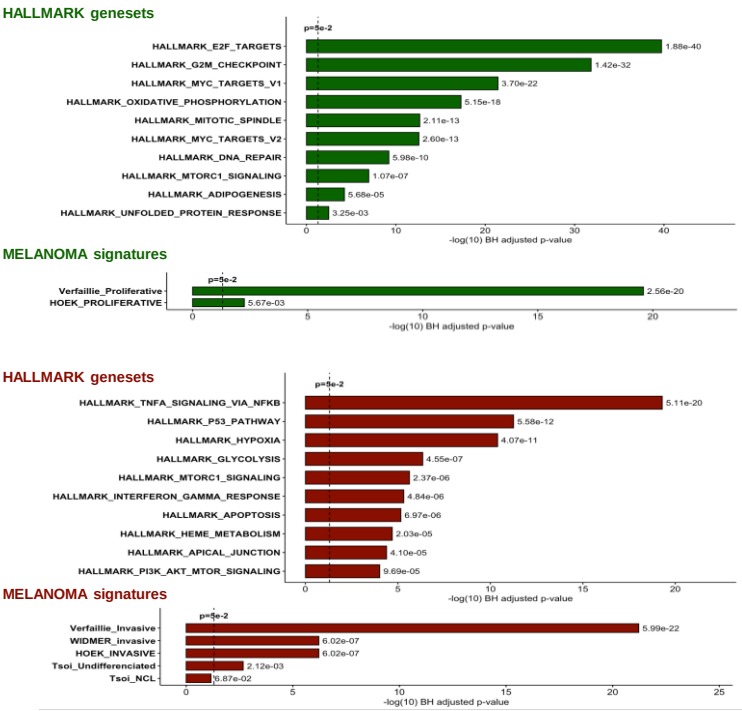


**G.**

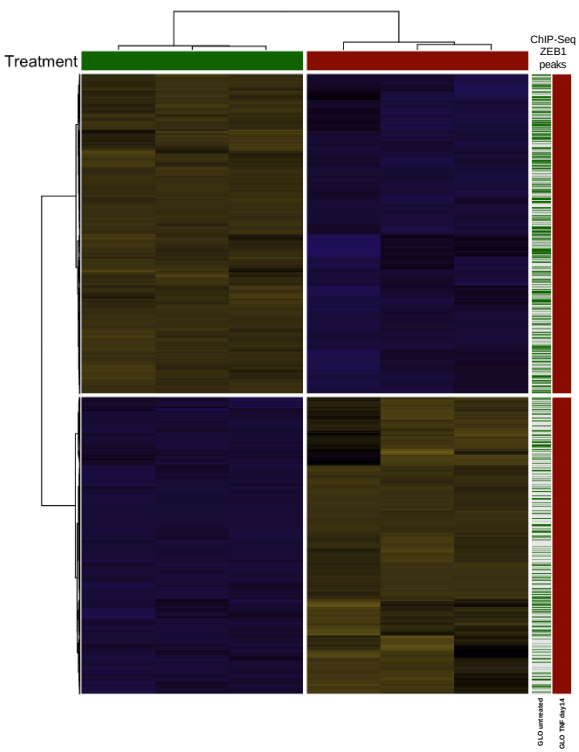


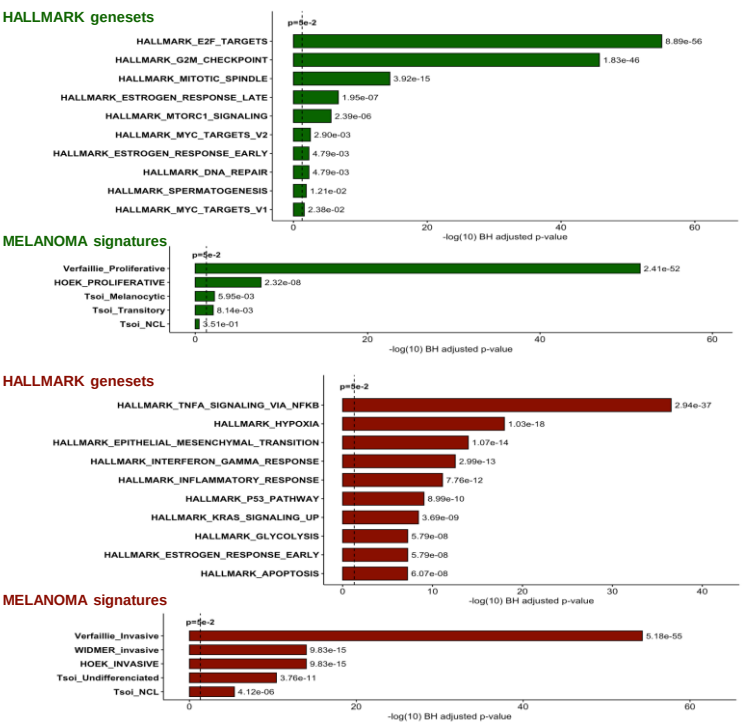

**Figure 2. ZEB1 ChIP-sequencing analyses in two melanoma cell lines**

ZEB1 ChIP sequencing was performed in GLO cells, untreated or after 14 days (D14) of TNFα treatment and in A375-AS3 (control) cells.

**A.** The number and size of peaks are indicated.

**B.** Venn diagram showing the overlap between peaks found in GLO cells untreated (green) or after 14 days of TNFα treatment (D14) (red) and in A375-AS3 cells (blue).

**C-D.** Localization of the peaks **(C)** and distance to the transcription start site **(D)**.

**E.** Top3 HOMER-identified enriched motifs in GLO after 14 days of TNFα treatment (50pb region centered on the peak). The associated p-values, the percentages of motif representation on target and background are indicated.

**F.** Heatmap of all genes presenting a ZEB1 binding peak in TNFα-treated cells at day 14. The most significantly enriched hallmarks and melanoma state signatures are indicated on the right. Clustering Ward.D2 / distance: Euclidean.

**G.** Integration of ChIP-Seq with RNA-seq data in GLO cells. Heatmap of DE genes presenting a ZEB1 peak in GLO cells after 14 days of TNFα treatment. Presence of a ZEB1 peak in the gene is indicated by a green line (untreated condition) or a red line (TNFα D14 condition) on the right. The most significantly enriched hallmarks and melanoma state signatures within down- and up-regulated genes in D14 versus untreated cells are indicated on the right.

Figure 3

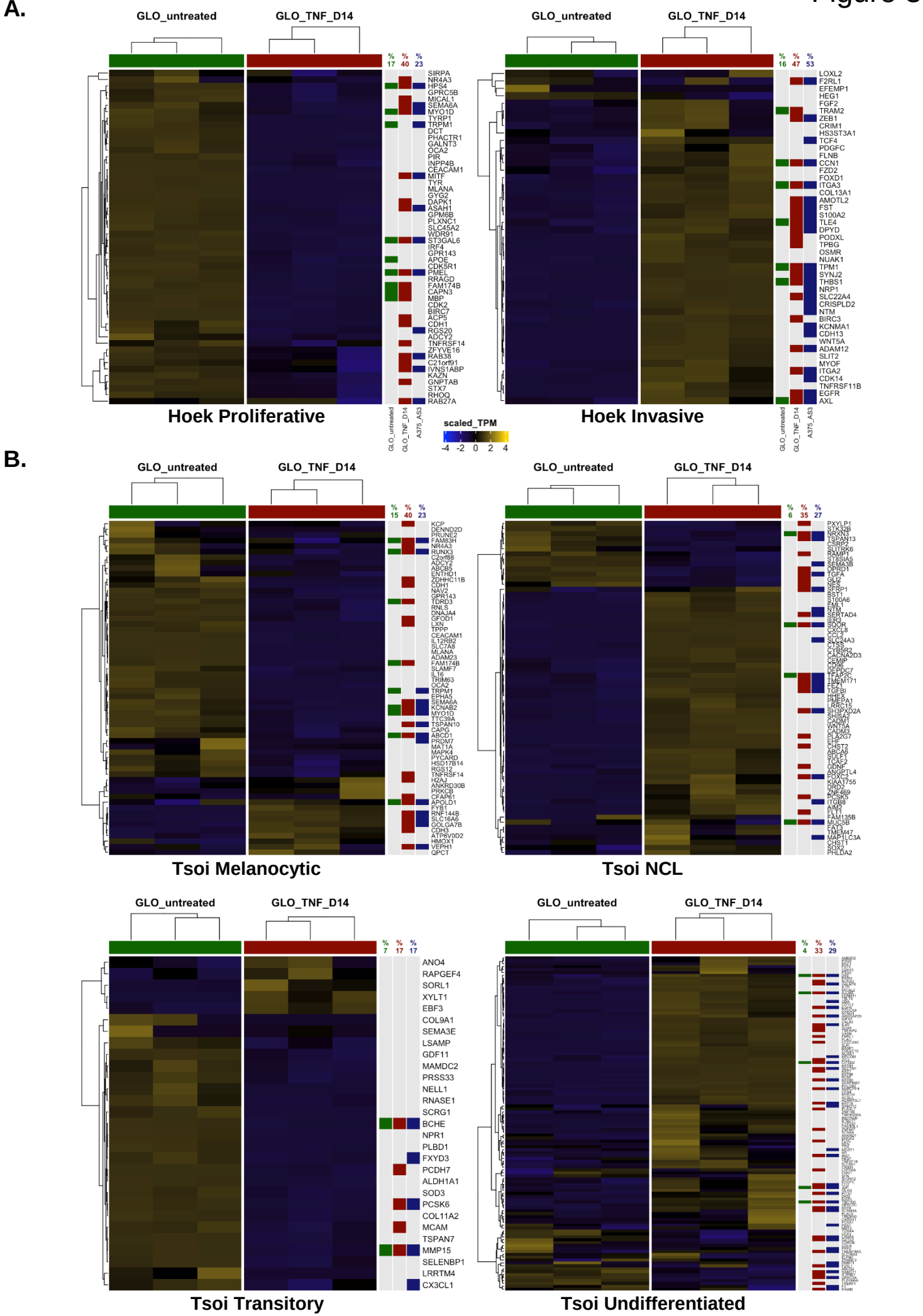
A.
GLO_untreated
GLO_TNF_D14
% 17 % 40 % 23
SIRPA
NR4A3
HPS4
GPRC5B
MICAL1
SEMA6A
MYO1D
TYRP1
TRPM1
DCT
PHACTR1
GALNT3
OCA2
PIR
INPP4B
CEACAM1
MITF
TYR
MLANA
GYG2
DAPK1
ASAH1
GPM6B
PLXNC1
SLC45A2
WDR91
ST3GAL6
IRF4
GPR143
APOE
CDK5R1
PMEL
RRAGD
FAM174B
CAPN3
MBP
CDK2
BIRC7
ACP5
CDH1
RGS20
ADCY2
TNFRSF14
ZFYVE16
RAB38
C21orf91
IVNS1ABP
KAZN
GNPTAB
STX7
RHOQ
RAB27A
Hoek Proliferative
GLO_untreated
GLO_TNF_D14
A375_AS3
% 16 % 47 % 53
LOXL2
F2RL1
EFEMP1
HEG1
FGF2
TRAM2
ZEB1
CRIM1
HS3ST3A1
TCF4
PDGFC
FLNB
CCN1
FZD2
FOXD1
ITGA3
COL13A1
AMOTL2
FST
S100A2
TLE4
DPYD
PODXL
TPBG
OSMR
NUAK1
TPM1
SYNJ2
THBS1
NRP1
SLC22A4
CRISPLD2
NTM
BIRC3
KCNMA1
CDH13
WNT5A
ADAM12
SLIT2
MYOF
ITGA2
CDK14
TNFRSF11B
EGFR
AXL
Hoek Invasive
GLO_untreated
GLO_TNF_D14
A375_AS3
scaled_TPM
-4 -2 0 2 4
B.
GLO_untreated
GLO_TNF_D14
% 15 % 40 % 23
KCP
DENND2D
PRUNE2
FAM83H
NR4A3
RUNX3
C2orf88
ADCY2
ABCB5
ENTHD1
ZDHHC11B
CDH1
NAV2
GPR143
TDRD3
RNLS
DNAJA4
GFOD1
LXN
TPPP
CEACAM1
IL12RB2
SLC7A8
MLANA
ADAM23
FAM174B
SLAMF7
IL16
TRIM63
OCA2
TRPM1
EPHA5
SEMA6A
KCNAB2
MYO1D
TTC39A
TSPAN10
CAPG
ABCD1
PRDM7
MAT1A
MAPK4
PYCARD
HSD17B14
RGS12
TNFRSF14
H2AJ
ANKRD30B
PRKCB
CFAP61
APOLD1
FYB1
RNF144B
SLC16A6
GOLGA7B
CDH3
ATP6V0D2
HMOX1
VEPH1
QPCT
Tsoi Melanocytic
GLO_untreated
GLO_TNF_D14
% 6 % 35 % 27
PXYLP1
STK32B
NRXN3
TSPAN13
CSRP2
SLITRK6
RAMP1
ST8SIA5
SEMA3B
OPRD1
TGFA
GLI2
NES
SFRP1
BST1
S100A6
EML1
NTM
SERTAD4
IER3
SOOR
CXCL8
CCL2
SLC24A3
CTSS
CYB5R2
CACNA2D3
CEMIP
CD96
DEPDC7
TFAP2C
TMEM171
FEZ1
TGFBI
HHEX
PMEPA1
LRRC15
SH3PXD2A
SHISA2
CADM1
WNT5A
CADM3
PLA2G7
EHF
CHST2
ABCA6
SULF1
TCAF2
GDNF
ANGPTL4
FOXC2
KIAA1755
DRD2
ZNF469
PCSK5
ITGB8
AIM2
FLT1
FAM135B
MUC5B
FAT3
TMEM47
MAP1LC3A
CHST1
SOX2
PHLDA2
Tsoi NCL
GLO_untreated
GLO_TNF_D14
% 7 % 17 % 17
ANO4
RAPGEF4
SORL1
XYLT1
EBF3
COL9A1
SEMA3E
LSAMP
GDF11
MAMDC2
PRSS33
NELL1
RNASE1
SCRG1
BCHE
NPR1
PLBD1
FXYD3
PCDH7
ALDH1A1
SOD3
PCSK6
COL11A2
MCAM
TSPAN7
MMP15
SELENBP1
LRRTM4
CX3CL1
Tsoi Transitory
GLO_untreated
GLO_TNF_D14
% 4 % 33 % 29
Tsoi Undifferentiated

**Figure 3. Specific analyses of ZEB1 binding on genes from melanoma cell state signatures**

Heatmap of genes from the melanoma signatures from Hoek et al. **(A)**, Tsoi et al. **(B)** in untreated or TNFα-treated GLO cells at day 14. The presence of a ZEB1 peak is indicated by a green (untreated), red (TNFα D14) or blue (A375-AS3 cells) square. The percentage of genes of the corresponding signature presenting a ZEB1 peak for each condition is indicated. Clustering Ward.D2 / distance: Euclidean.

A.

Figure 4

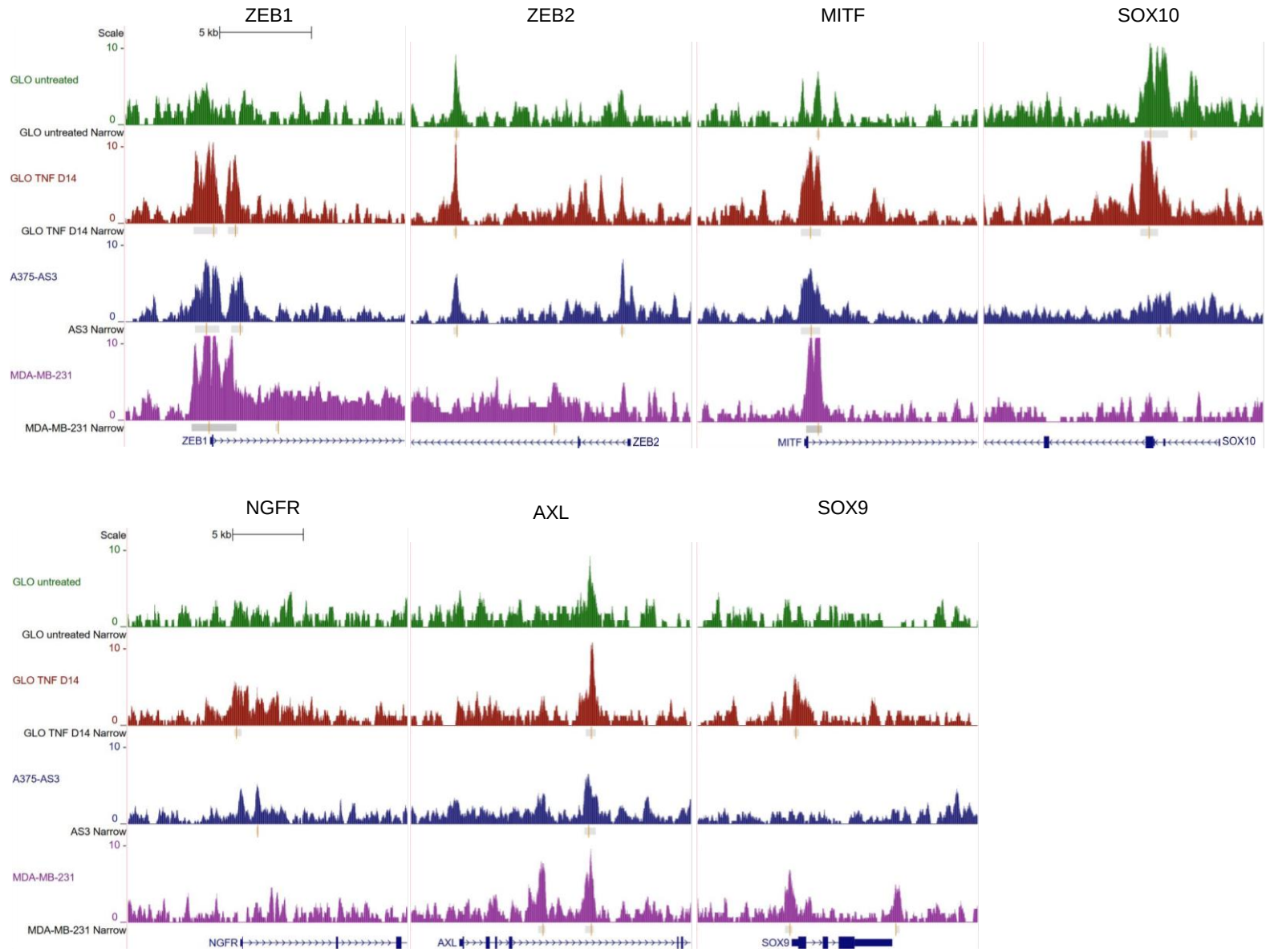
ZEB1
ZEB2
MITF
SOX10
NGFR
AXL
SOX9
Scale
5 kb
GLO untreated
GLO untreated Narrow
GLO TNF D14
GLO TNF D14 Narrow
A375-AS3
AS3 Narrow
MDA-MB-231
MDA-MB-231 Narrow

B.

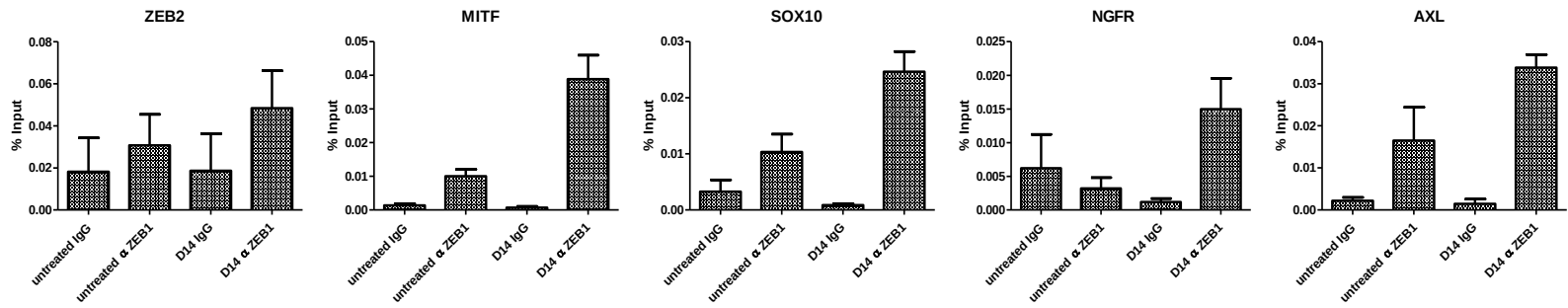
ZEB2
MITF
SOX10
NGFR
AXL
% Input
untreated IgG
untreated α ZEB1
D14 IgG
D14 α ZEB1

C.

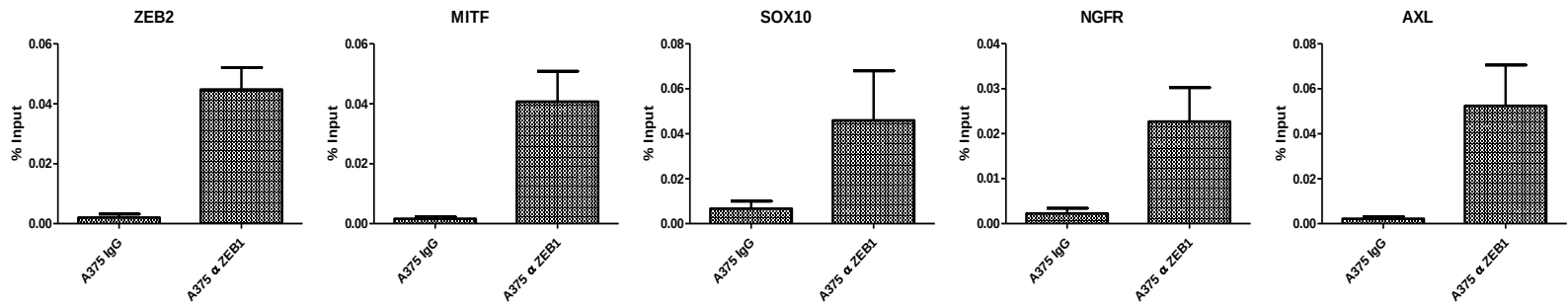
ZEB2
MITF
SOX10
NGFR
AXL
% Input
A375 IgG
A375 α ZEB1

**Figure 4. Validation by ChIP-qPCR of ZEB1 binding on the promoters of lineage-specific major markers of melanoma cell states.**

**A.** UCSC genome browser captures showing ZEB1 binding peaks in *ZEB1*, *ZEB2*, *MITF*, *NGFR*, *AXL*, *SOX10* and *SOX9* promoters in untreated or TNFα-treated GLO cells at day 14 (TNF D14), A375-AS3 cells and MDA-MB-231 cells. Significantly enriched peaks are marked by a grey square and red line.

**B-C.** ZEB1 ChIP-qPCR on *ZEB2*, *MITF*, *NGFR*, *AXL*, and *SOX10* promoters in GLO cells treated with TNFα for 14 days (D14) (**B**) and A375 cells (**C**). Anti-ZEB1 (α ZEB1) or control IgG were used for the IP. Relative promoter enrichment was normalized against chromatin inputs (n = 3). Data are shown as the mean ± SEM.

Figure 5

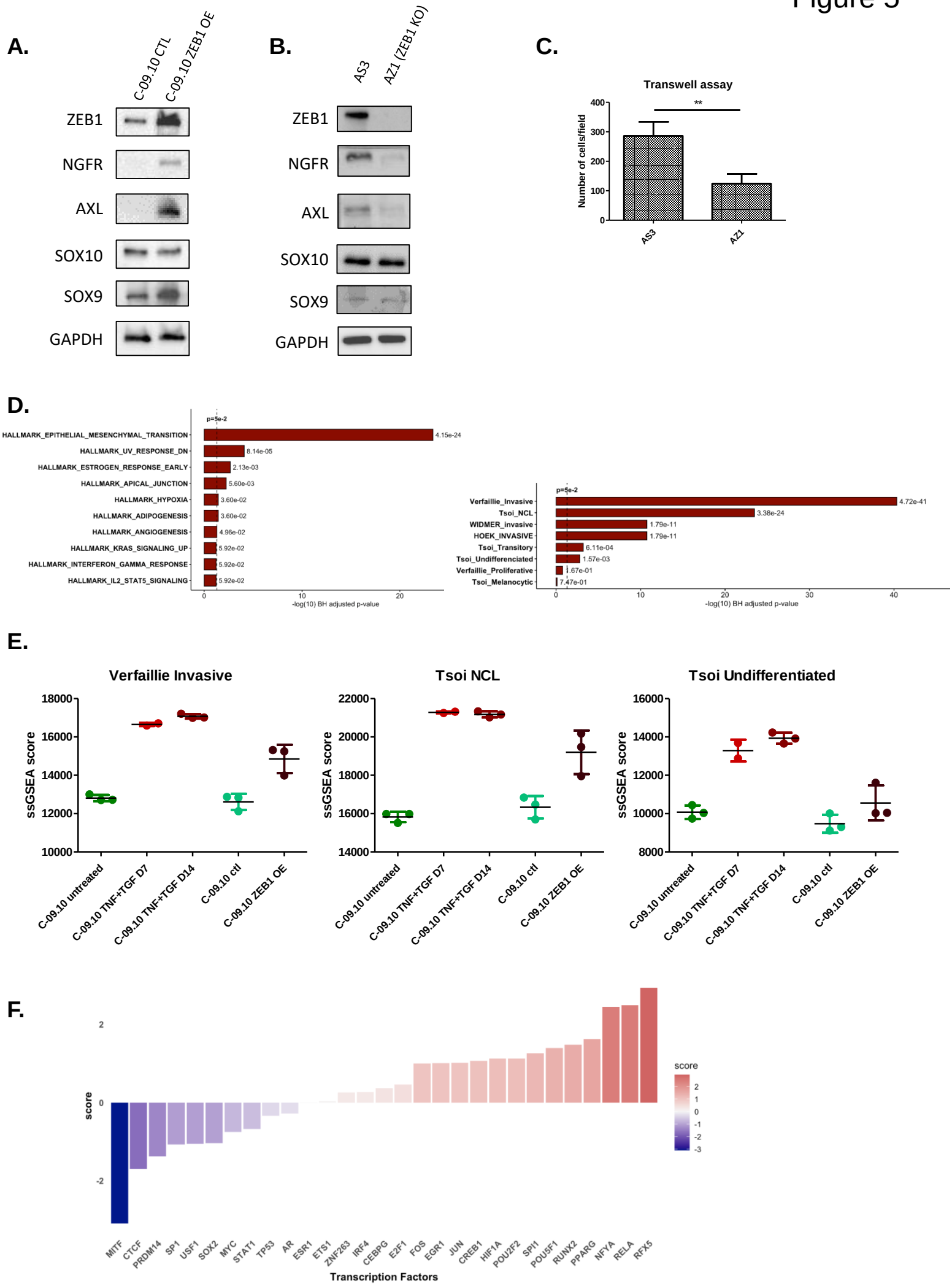
A.
C-09.10 CTL
C-09.10 ZEB1 OE
ZEB1
NGFR
AXL
SOX10
SOX9
GAPDH
B.
AS3
AZ1 (ZEB1 KO)
ZEB1
NGFR
AXL
SOX10
SOX9
GAPDH
C.
Transwell assay
Number of cells/field
400
300
200
100
0
**
AS3
AZ1
D.
p=5e-2
HALLMARK_EPITHELIAL_MESENCHYMAL_TRANSITION 4.15e-24
HALLMARK_UV_RESPONSE_DN 8.14e-05
HALLMARK_ESTROGEN_RESPONSE_EARLY 2.13e-03
HALLMARK_APICAL_JUNCTION 5.60e-03
HALLMARK_HYPOXIA 3.60e-02
HALLMARK_ADIPOGENESIS 3.60e-02
HALLMARK_ANGIOGENESIS 4.96e-02
HALLMARK_KRAS_SIGNALING_UP 5.92e-02
HALLMARK_INTERFERON_GAMMA_RESPONSE 5.92e-02
HALLMARK_IL2_STAT5_SIGNALING 5.92e-02
0
10
20
-log(10) BH adjusted p-value
p=5e-2
Verfaillie_Invasive 4.72e-41
Tsoi_NCL 3.38e-24
WIDMER_invasive 1.79e-11
HOEK_INVASIVE 1.79e-11
Tsoi_Transitory 6.11e-04
Tsoi_Undifferenciated 1.57e-03
Verfaillie_Proliferative 1.67e-01
Tsoi_Melanocytic 7.47e-01
0
10
20
30
40
-log(10) BH adjusted p-value
E.
Verfaillie Invasive
Tsoi NCL
Tsoi Undifferentiated
ssGSEA score
C-09.10 untreated
C-09.10 TNF+TGF D7
C-09.10 TNF+TGF D14
C-09.10 ctl
C-09.10 ZEB1 OE
F.
score
2
0
-2
MITF
CTCF
PRDM14
SP1
USF1
SOX2
MYC
STAT1
TP53
AR
ESR1
ETS1
ZNF263
IRF4
CEBPG
E2F1
FOS
EGR1
JUN
CREB1
HIF1A
POU2F2
SPI1
POU5F1
RUNX2
PPARG
NFYA
RELA
RFX5
Transcription Factors

**Figure 5: ZEB1-dependent regulation of markers of melanoma cell states in gain or loss of function models.**

**A-B.** Western blot analyses of phenotype markers (ZEB1, NGFR, AXL, SOX10, SOX9) in C-09.10 cells with ZEB1 over-expression (ZEB1) (**A**) and in A375 control (AS3) or *ZEB1* knocked-out (AZ1) clones (**B**). (n = 3).

**C.** Transwell migration assays in A375-AS3 and A375-AZ1 ZEB1 knocked-out cells. Cells were fixed after 24 h, the number of migrating cells is plotted. Two-tailed ratio paired t-tests (n = 4). Differences were considered statistically significant at $*P \leq 0.05$, $**P < 0.01$ and $***P < 0.001$. ns (non-significant) means $P > 0.05$.

**D.** RNA-seq analyses of C-09.10 cells upon ZEB1 over-expression (ZEB1 OE). The most significant hallmarks and melanoma signatures enriched in up-regulated genes in ZEB1 OE are indicated.

**E.** ssGSEA scores of invasive, NCL and undifferentiated melanoma signatures are plotted in C-09.10 cells upon ZEB1 over-expression or upon TNFα + TGFβ treatment at day 7 and day 14 for comparison.

**F.** Inference of transcription factors (TF) activity in gene expression data using VIPER algorithm. Barplot of DoRothEA TF Normalized Enrichment Score (NES) comparing control versus ZEB1 OE C-09.10 cells.

Figure 6

**A.**

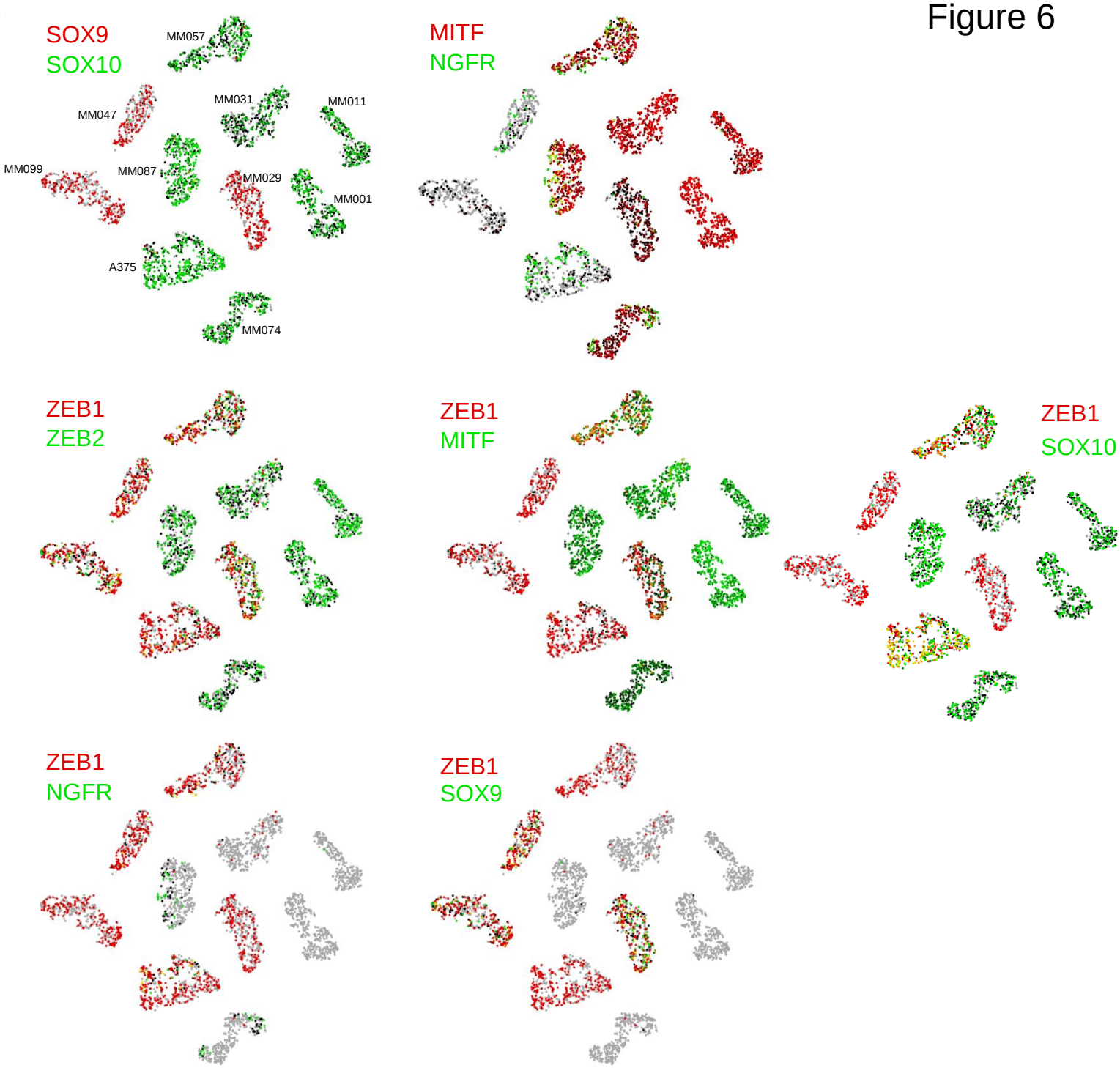
SOX9
SOX10
MM057
MM047
MM031
MM011
MM099
MM087
MM029
MM001
A375
MM074
MITF
NGFR
ZEB1
ZEB2
ZEB1
MITF
ZEB1
SOX10
ZEB1
NGFR
ZEB1
SOX9

**B.**

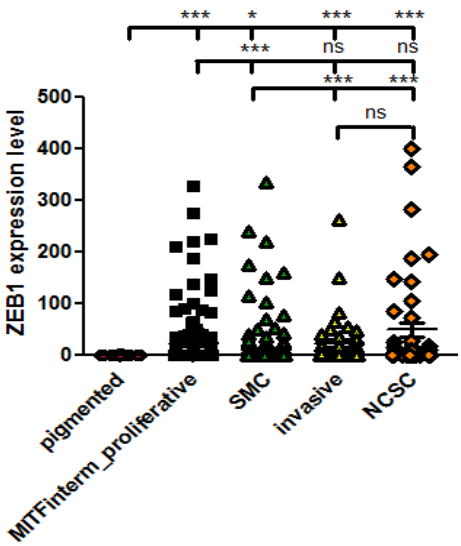
ZEB1 expression level
500
400
300
200
100
0
***
*
***
***
***
ns
ns
***
***
ns
pigmented
MITFinterm_proliferative
SMC
invasive
NCSC

**Figure 6. ZEB1 expression in public single-cell RNA-seq dataset of melanoma cell lines and PDX**

**A.** t-SNE visualizations of single-cell RNA-seq data of 10 melanoma cell lines from *Wouters et al*. The expression levels of ZEB1, MITF, SOX9, SOX10, ZEB2 and NGFR are indicated. The expression levels of the 2 corresponding genes are indicated in red and green, respectively, cells expressing both genes appear in yellow. Cells expressing low levels of corresponding genes appear dark.

**B.** ZEB1 expression levels in the different cell states defined by *Rambow et al., 2018* in single cell RNA-seq data of melanoma patient-derived xenografts (PDXs). P values were determined by Mann-Whitney test. Differences were considered statistically significant at $*P \leq 0.05$, $**P < 0.01$ and $***P < 0.001$. ns (non-significant) means $P > 0.05$.

Figure 7

**A.**

**Patient #A – Zeb1 low**

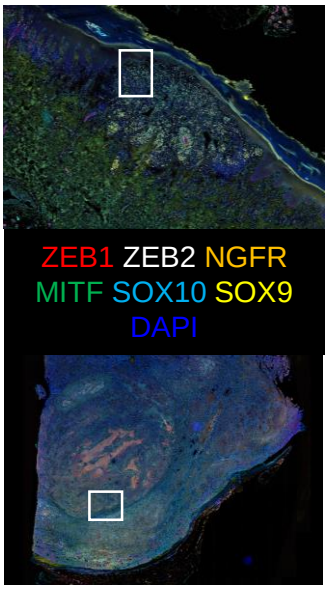


**Patient #B – Zeb1 high**

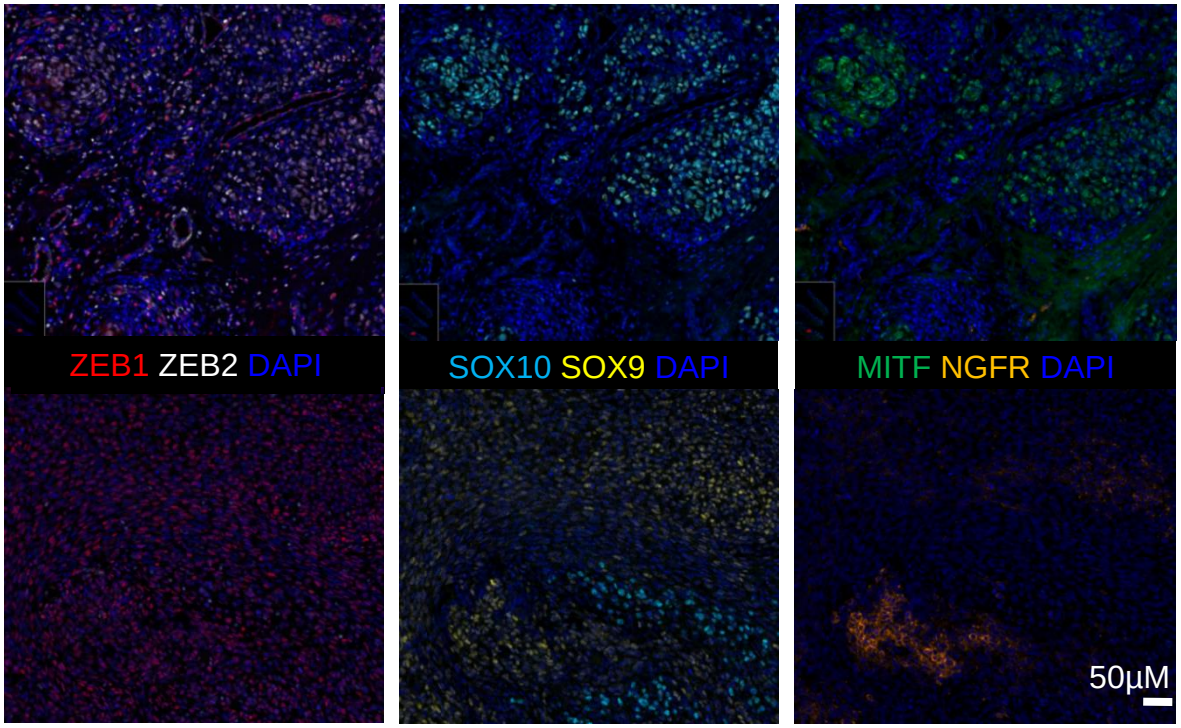


**B.**

**Patient #C – ZEB1 low**

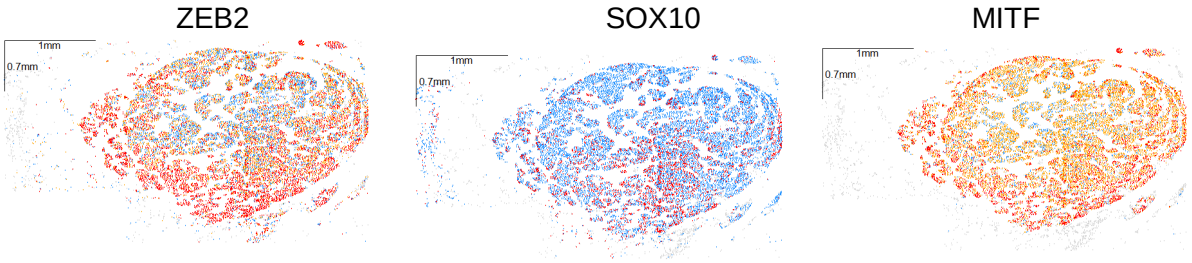


**C.**

**Patient #D – ZEB1 high clone**

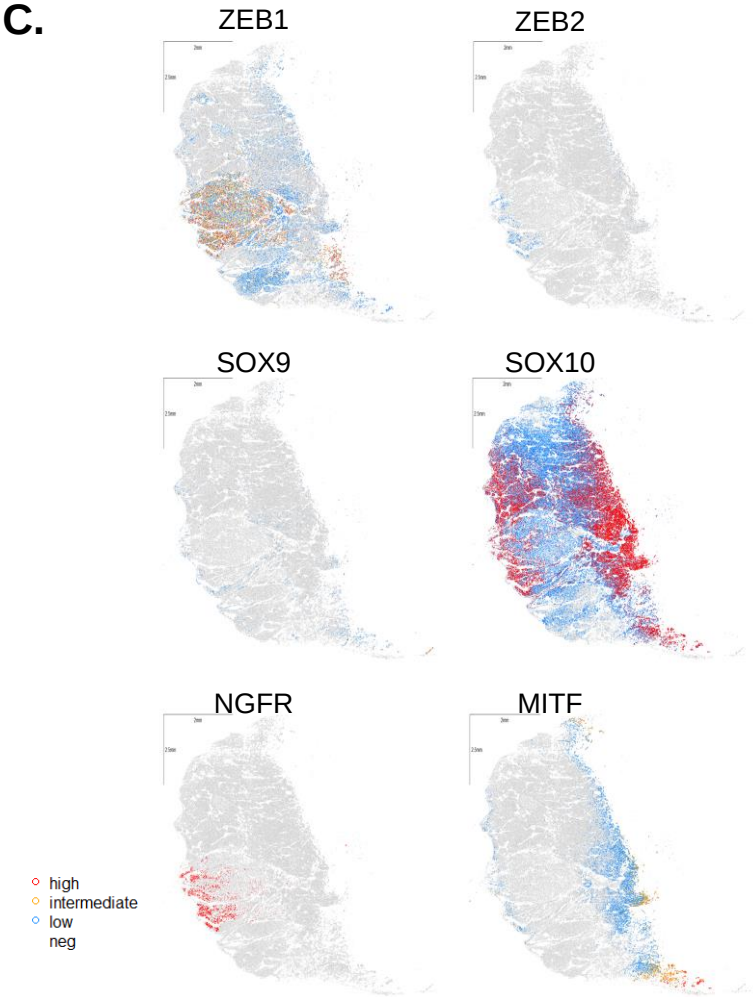


**D.**

**Patient #B – ZEB1 high**

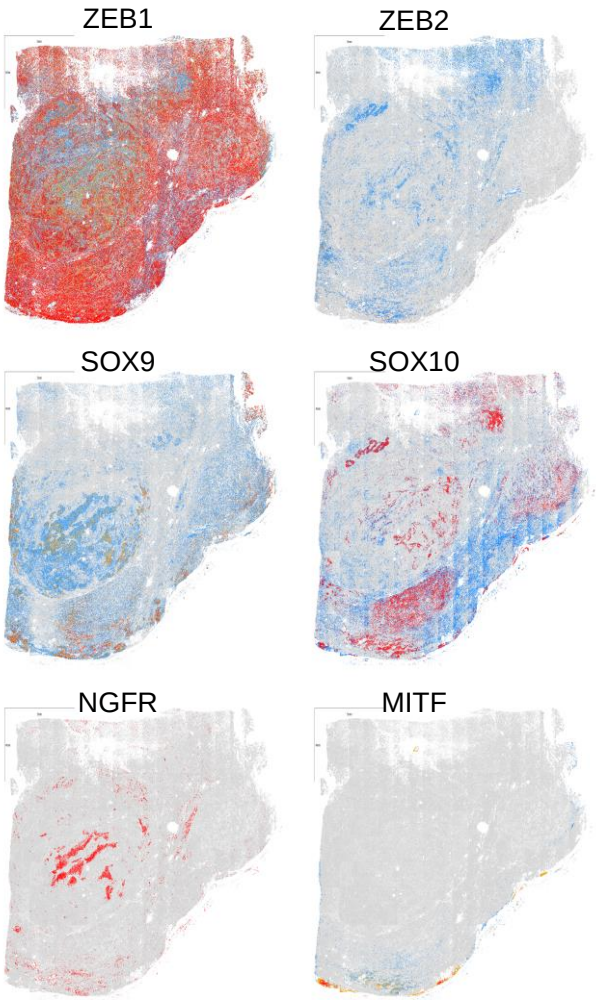

**Figure 7. Single-cell spatial analyses of markers of melanoma cell states according to ZEB1 status in melanoma samples.**

**A.** 7-color multiplexed immunofluorescence analyses of human melanoma samples with ZEB1 (red), ZEB2 (white), SOX10 (blue), SOX9 (yellow), NGFR (orange), MITF (green) and DAPI. Representative pictures of a ZEB1$^{low}$ (top) and a ZEB1$^{high}$ (bottom) cutaneous melanoma showing antagonistic expression of ZEB1 and ZEB2, MITF and NGFR, and SOX10 and SOX9.

**B-C-D.** Reconstruction of three representative heterogeneous tumors as whole slides: a ZEB1$^{low}$ (**B**), and two ZEB1$^{high}$ tumors (**C-D**). Each dot represents a cell. The expression levels of ZEB1, ZEB2, MITF and SOX9 are indicated in red (high), yellow (intermediate), blue (low) and grey (not expressed). SOX10 display 3 levels of expression defined as high, low and not expressed; and NGFR display only 2 levels of expression defined as high and not expressed.

Figure 8

A.

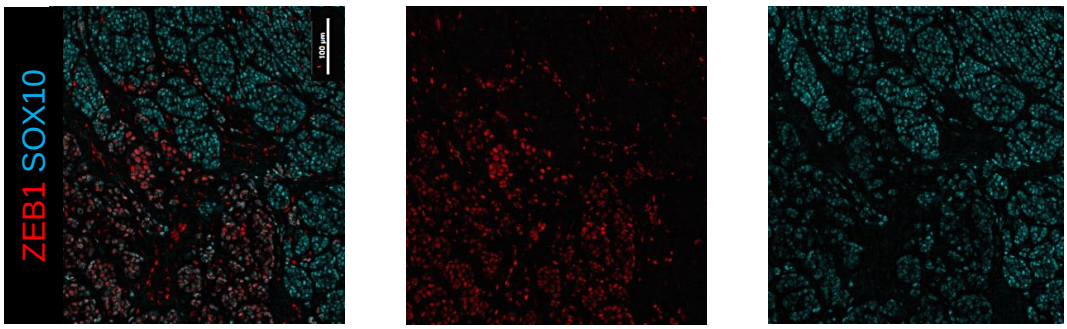


B.

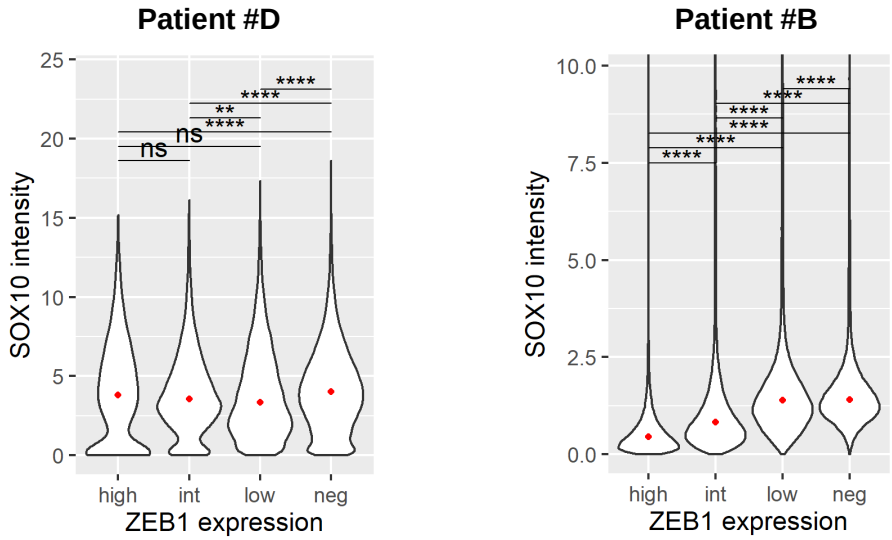


C.

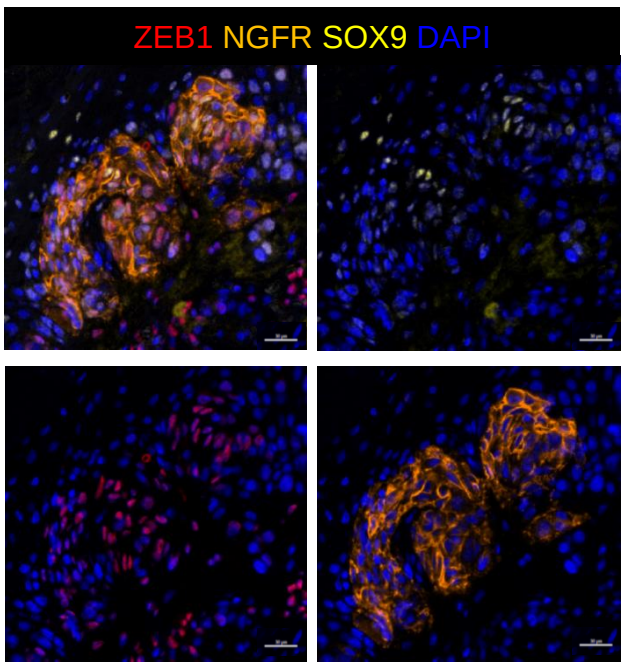


D.

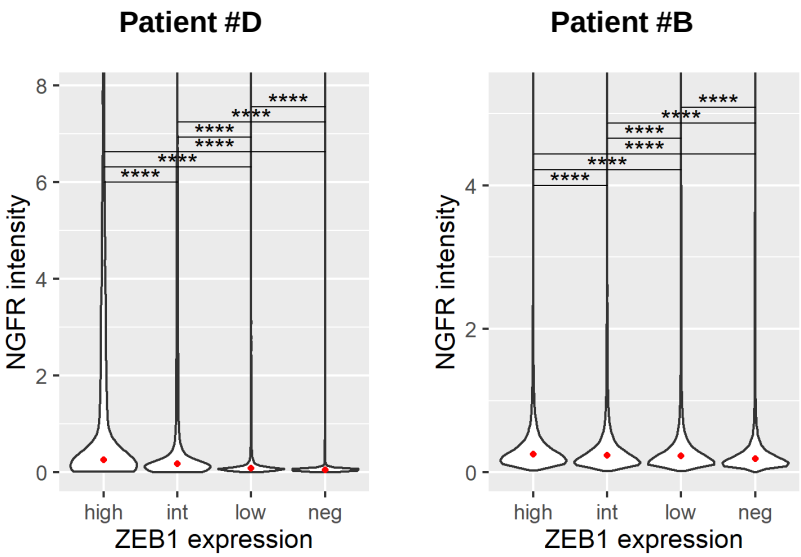


E.

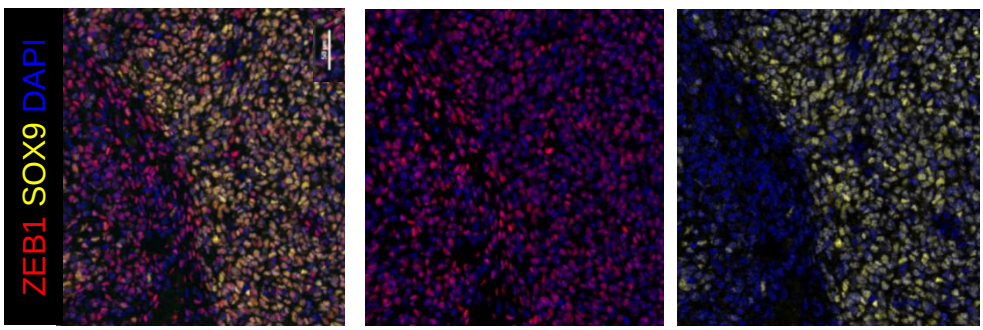


F.

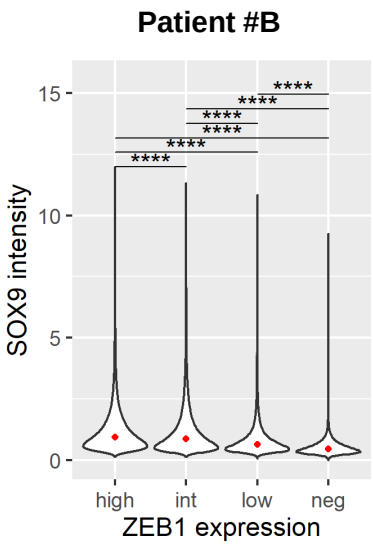

**Figure 8. ZEB1 antagonistic expression with SOX10 and co-expression with NGFR and SOX9 within melanoma lesions.**

**A.** Representative pictures of ZEB1 and SOX10 staining showing antagonistic expression of ZEB1 and SOX10 in the ZEB1$^{high}$ clone from Patient #D.

**B.** Violin plots showing the expression levels of SOX10 for cells grouped with respect to their ZEB1 expression status (high, intermediate, low or not expressed) in two representative ZEB1$^{high}$ melanoma cases.

**C.** Representative pictures of ZEB1, NGFR and/or SOX9 staining showing co-expression of ZEB1 with NGFR and/or SOX9.

**D.** Violin plots showing the expression levels of NGFR for cells grouped with respect to their ZEB1 expression status (high, intermediate, low or not expressed) in two representative ZEB1$^{high}$ melanoma cases.

**E.** Representative pictures of ZEB1 and SOX9 staining showing co-expression of ZEB1 with SOX9.

**F.** Violin plots showing the expression levels of SOX9 for cells grouped with respect to their ZEB1 expression status (high, intermediate, low or not expressed) in one representative ZEB1$^{high}$ melanoma.

The median is shown with a red dot. P values were determined by Mann-Whitney test with Bonferroni correction **(B, D, F)**. Differences were considered statistically significant at $^{*}P \leq 0.05$, $^{**}P < 0.01$ and $^{***}P < 0.001$. ns (non-significant) means $P > 0.05$.